

NAVAL POSTGRADUATE SCHOOL

Monterey, California



THESIS

**ANTI-SHIP MISSILE DEFENSE
AND THE FREE ELECTRON LASER**

by

Paul A. Herbert

December 1998

Thesis Advisor:
Second Reader:

William B. Colson
Robert L. Armstead

19990212031

Approved for public release; distribution is unlimited.

Preceding Pages Blank

DEG QUALITY INSPECTED 1

REPORT DOCUMENTATION PAGE

Form Approved
OMB No. 0704-0188

Public reporting burden for this collection of information is estimated to average 1 hour per response, including the time for reviewing instruction, searching existing data sources, gathering and maintaining the data needed, and completing and reviewing the collection of information. Send comments regarding this burden estimate or any other aspect of this collection of information, including suggestions for reducing this burden, to Washington Headquarters Services, Directorate for Information Operations and Reports, 1215 Jefferson Davis Highway, Suite 1204, Arlington, VA 22202-4302, and to the Office of Management and Budget, Paperwork Reduction Project (0704-0188) Washington DC 20503.

1. AGENCY USE ONLY (Leave blank)	2. REPORT DATE December 1998	3. REPORT TYPE AND DATES COVERED Master's Thesis
4. TITLE AND SUBTITLE Anti-Ship Missile Defense And The Free Electron Laser		5. FUNDING NUMBERS
6. AUTHOR(S) Herbert, Paul A.		
7. PERFORMING ORGANIZATION NAME(S) AND ADDRESS(ES) Naval Postgraduate School Monterey, CA 93943-5000		8. PERFORMING ORGANIZATION REPORT NUMBER
9. SPONSORING / MONITORING AGENCY NAME(S) AND ADDRESS(ES)		10. SPONSORING / MONITORING AGENCY REPORT NUMBER
11. SUPPLEMENTARY NOTES The views expressed in this thesis are those of the author and do not reflect the official policy or position of the Department of Defense or the U.S. Government.		
12a. DISTRIBUTION / AVAILABILITY STATEMENT Approved for public release; distribution is unlimited.		12b. DISTRIBUTION CODE
13. ABSTRACT <p>In order to improve ship self-defense against sea-skimming missiles, several concepts, such as the free electron laser, high-power microwaves, and the Phalanx gun system are reviewed and evaluated in this thesis. Phalanx computer simulations show that Phalanx is an inadequate means of protection. High-power microwaves are found to damage electronics, but calculations show limitations due to diffraction and the possibility of shielding. This thesis evaluates several damage mechanisms caused by the free electron laser's ultra-short picosecond pulse. Theories and experiments predicting the laser damage from short picosecond pulses are reviewed and applied to the fel weapon design. It is found that there may be a significant advantage to the ultra-short pulse format of an FEL weapon; as a result, new experiments are planned. As MW FELs are not yet a reality, this thesis uses computer simulations to explore FEL operation for many values of the electron pulse length, peak current and cavity desynchronization in order to explain recent Thomas Jefferson National Accelerator Facility (TJNAF) experimental observations of high average power.</p>		
14. SUBJECT TERMS Free Electron Laser, Directed Energy Weapons, Ship Defense		15. NUMBER OF PAGES 88
16. PRICE CODE		
17. SECURITY CLASSIFICATION OF REPORT Unclassified	18. SECURITY CLASSIFICATION OF THIS PAGE Unclassified	19. SECURITY CLASSIFICATION OF ABSTRACT Unclassified
20. LIMITATION OF ABSTRACT UL		

Approved for public release; distribution is unlimited

ANTI-SHIP MISSILE DEFENSE AND THE FREE ELECTRON LASER

Paul A. Herbert
Lieutenant, United States Navy
B.S., United States Naval Academy, 1989

Submitted in partial fulfillment of the
requirements for the degree of

MASTER OF SCIENCE IN APPLIED PHYSICS

from the

NAVAL POSTGRADUATE SCHOOL
December 1998

Author:

Paul A. Herbert

Paul A. Herbert

Approved By:

W. B. Colson

William B. Colson, Thesis Advisor

Robert L. Armstead

Robert L. Armstead, Second Reader

William Maier

William Maier, Chair
Department of Physics

ABSTRACT

In order to improve ship self-defense against sea-skimming missiles, several concepts, such as the free electron laser, high-power microwaves, and the Phalanx gun system are reviewed and evaluated in this thesis. Phalanx computer simulations show that Phalanx is an inadequate means of protection. High-power microwaves are found to damage electronics, but calculations show limitations due to diffraction and the possibility of shielding. This thesis evaluates several damage mechanisms caused by the free electron laser's ultra-short picosecond pulse. Theories and experiments predicting the laser damage from short picosecond pulses are reviewed and applied to the fel weapon design. It is found that there may be a significant advantage to the ultra-short pulse format of an FEL weapon; as a result, new experiments are planned. As MW FELs are not yet a reality, this thesis uses computer simulations to explore FEL operation for many values of the electron pulse length, peak current and cavity desynchronization in order to explain recent Thomas Jefferson National Accelerator Facility (TJNAF) experimental observations of high average power.

TABLE OF CONTENTS

I. INTRODUCTION.....	1
A. BACKGROUND	1
B. PASSIVE MEANS OF PROTECTION.....	3
1. Decoys	4
2. Camouflage	4
3. Doctrine/Tactics.....	4
C. ACTIVE MEANS OF PROTECTION	5
II. KINETIC ENERGY WEAPONS APPROACH	7
A. CLOSE-IN-WEAPON-SYSTEM (CIWS)	7
B. ANTI-MISSILE MISSILES	11
III. DIRECTED ENERGY WEAPONS APPROACH.....	15
A. BACKGROUND	15
B. HIGH POWER MICROWAVES (HPM)	16
1. Background	16
2. Source Selection	19
3. Propagation.....	20
4. Effects.....	25
5. Hardening	27
6. Conclusion.....	30
C. LASERS	30
1. Background	30
2. Atmospheric Propagation	32
3. Conclusion.....	39
IV. FEL THEORY.....	41
A. BASIC OPERATION	41
B. PENDULUM EQUATION.....	43
C. WAVE EQUATION.....	46
D. LOW GAIN FEL	50
E. SHORT PULSE EFFECTS	54
F. DESYNCHRONISM EFFECTS	56
G. LIMIT CYCLE BEHAVIOR	58
V. LASER MATTER INTERACTION	61
A. CONTINUOUS WAVE	61
B. SHORT PULSE EFFECTS	62
C. ULTRA-SHORT PULSE EFFECTS	63
VI. TJNAF FEL.....	67
VII. CONCLUSIONS.....	73
LIST OF REFERENCES.....	75
INITIAL DISTRIBUTION LIST	79

I. INTRODUCTION

A. BACKGROUND

For the greater part of the past four decades, our military has been concerned with an adversary of equal military prowess, a military that could and would stand toe to toe with our military. Therefore, in the past, the conflict simulations used most often for the purposes of determining our military readiness consisted of two countries massing their forces to overwhelm each other. The designs of our current warships were derived from the results of these simulations and existing technologies. Most of the weapon systems onboard USN warships today, were designed to fight an equal or greater force upon the open ocean.

However, the world is not a static system, but it is rather a continuously changing system of requirements and demands. As the world changes, traditional methodology may not work for many situations that can arise. An example is the collapse of the Soviet Union. The Cold War is now over and the chances that our military will encounter an equal military in the near future are slim at best. Even so, we can not concentrate our efforts entirely on threats from smaller Third World countries. China is modernizing its already highly capable military and future United States-China relations may deteriorate and again threaten large-scale naval conflicts.

Some lesser-developed countries have sought to gain equal footing in the world's hierarchy via military means. Many Third World countries now possess capable weapons systems that include chemical, biological, nuclear and high-tech components.

Changing world requirements and the need for a strong flexible military has forced the Navy to re-address its role. Rather than fighting in the open ocean, the Navy's role is now primarily supporting troops ashore by operating in the littoral region alone with little or no support, or possibly in conjunction with foreign militaries.

Ideally therefore, the navy needs ships that are capable of successfully engaging the enemy asea and ashore, while still being able to defend themselves from any attack. In practice however, it has been shown that although our modern warships are capable of attack they lack adequate defense against modern anti-ship missiles, which are now possessed by several Third World countries. A couple of illustrative examples are the sinking of the *HMS Sheffield*, and the near sinking of the *USS Stark* by the low-flying, sea-skimming Exocet missile. As anti-ship missiles are become cheaper, smarter, longer in range and proliferate into the Third World, better defensive weapons are needed.

This thesis concentrates on methods of ship air defense. A simulation shows that the Navy's Close-In-Weapon-System (CIWS) allows sea-skimming missiles to approach within a few hundred meters of the ship causing significant debris to hit the ship. High-power microwaves are evaluated as a means of destroying the missile electronics, but are found to be limited due to the diffraction of long wavelength radiation. Several damage mechanisms caused by the free electron laser (FEL) are evaluated. The ultra-short, high peak power laser pulses from the FEL are shown to not cause vapor blowoff or spalling, but do decrease the damage threshold fluence. Experiments and theory indicate that the ultra-short FEL pulses may increase damage by as much as a factor of 10. Finally,

simulations of the Jefferson Lab FEL describe recent experimental results of high average power.

B. PASSIVE MEANS OF PROTECTION

For a ship to be successful against an anti-ship missile, it must render the inbound missile ineffective, which can be done by physically destroying or impairing the missile, blinding its sensors, or attacking the missile's internal electronics. Blinding a missile's sensors can be done by attacking the missile's sensors or deceiving the sensors. The Navy currently has well established programs for the research and development of deception devices. It is not the purpose of this paper to delve into those methods other than to mention them briefly for completeness.

1. Decoys

Decoys are systems that can be deployed away from the object to be protected. In the case of ship protection, the decoys emulate the ship in some manner that would confuse an inbound weapon. They can be passive, like CHAFF, or active, giving off RF or thermal signals that are intended to confuse the inbound missile. These systems are generally very cheap and work well in combination with other ship defense systems.

2. Camouflage

Camouflage is a means of disguising an object to make it more difficult to detect. The Navy has hidden ships with the use of different paint schemes and colors to make visual identification more difficult. When anti-ship missiles use RF seekers rather than visual or electro-optical seekers, the ships are no longer hidden. Therefore, the Navy has aggressively pursued concepts that will reduce the radar cross section for new ships. This

includes investigations into the use of radar absorbent materials (RAM) and stealth technology to reduce a ship's radar signature. Stealth technology and RAM are very promising solutions that are being implemented in the design of new ships as well as on existing ships. This solution might be effective against current and near future anti-ship missile and ship detection methods. However, RAM is only effective against RF, with new advancements in missile seeker technology, including impulse radar and hyperspectral imaging, RAM will become an ineffective means for camouflage.

3. Doctrine/Tactics

The last means of passive ship defense is the use of training and tactics. By assessing scenarios that a ship may encounter, a list of limitations for ship safety can be produced. By accepting these limitations, a set of tactics can be constructed that would prevent a ship from encountering the scenarios that would endanger the ship unnecessarily. For example, it has been shown that the Navy standard missile is very effective against long-range, non-maneuvering, anti-ship missiles. Therefore, a doctrine can be established that keeps all enemy missile launchers at a safe distance. This is a cheap, effective means of protection, provided the limitations do not prevent mission accomplishment. Unfortunately, current Navy missions require ships to operate within the littoral region, which allows the possibility of having launchers inside of the minimum acceptable range.

C. ACTIVE MEANS OF PROTECTION

The other methods of anti-ship missile defense focus on attacking the missile. A system achieves a "kill" by successfully defeating a threat missile. These missile "kills"

can be further broken down into two categories, hard kill and soft kill. The preferred method of stopping an inbound missile is to achieve a hard kill: large-scale physical destruction, normally associated with physically destroying the missile. A less desirable but still a valid method of destruction is soft kill where mission-critical components are disabled while the target body remains largely undamaged. This is usually the result of blinding the sensors by attacking the internal electronics [1]. There are currently two basic methods of achieving kills on incoming missiles, they are kinetic energy and directed energy weapons.

II. KINETIC ENERGY WEAPONS APPROACH

A. CLOSE-IN-WEAPON-SYSTEM (CIWS)

The kinetic energy approach of destroy an incoming missile is normally thought to be a hard kill mechanism. The idea is to hit the incoming missile with a physical object and thereby destroy the inbound missile. The Close-in-Weapon-System (CIWS) aboard most surface ships was designed to achieve a hard kill by striking the incoming missile with multiple penetrators, with the goal of detonating the missile. The main advantages of the CIWS are 1) small size and low weight, 2) tested and in production, and 3) cheapest solution. However being a mechanical system, using explosive cartridges to propel the shells, the CIWS is prone to vibrational inaccuracies. In addition to these inaccuracies, the CIWS has a limited effective range of approximately two kilometers. Therefore, the CIWS may destroy the missile at such a close range, that large pieces of the missile may still have enough momentum to reach the ship and cause serious damage. The final disadvantage to be pointed out is the limited magazine of the CIWS.

For comparison in ship defense systems, the effectiveness CIWS in striking and subsequently destroying an inbound missile before impact was investigated via computer simulations. The first step was to calculate, as shown in Figure (1), the probability of hitting the missile vs. the missile range. Given the effective range of the CIWS, this plot was started at a missile range of 2000 m. It can be clearly seen, with this simulation of

the phalanx gun system, that a missile is likely to get close to the ship before being struck by a single penetrator.

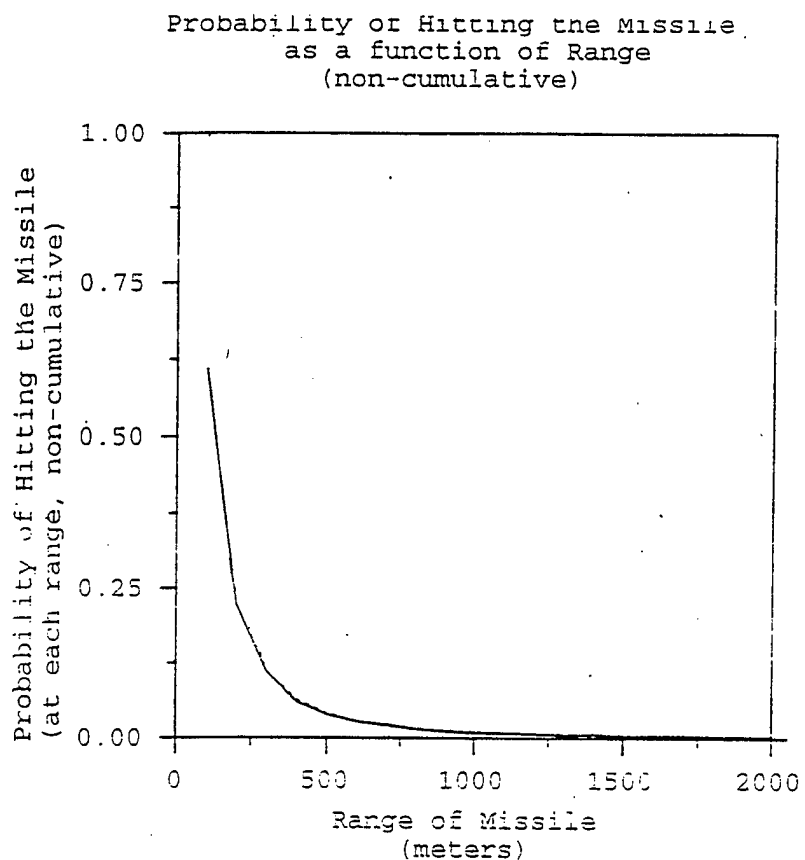


Figure 1. Probability of Hitting Inbound Missile vs. Range

The next simulation in the determination of the CIWS' effectiveness in destroying an incoming missile was the cumulative hits vs. missile range, see Figure (2). For this simulation, it was assumed that the missile did not maneuver and traveled at only 400 m/s. Combing the data from Figure (2) with the assumption that it takes 10 hits to destroy a missile, the kill range can be calculated. The typical kill range was determined

to be 100-200 meters from the ship [2]. Therefore, the phalanx is capable of destroying a missile as designed. However, the debris from the missile has a strong possibility.

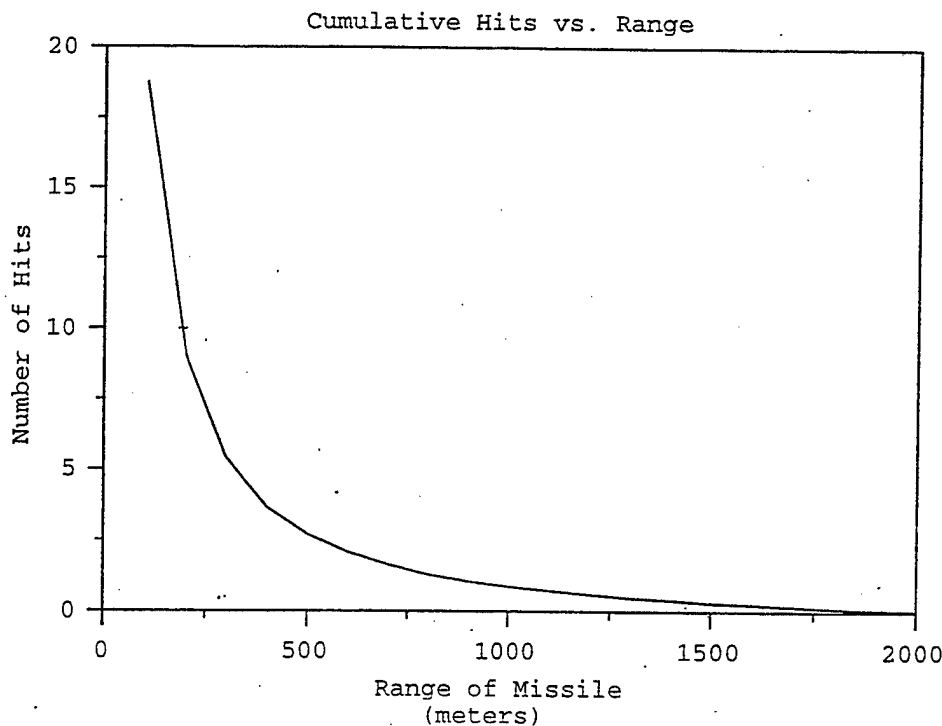


Figure 2. Cumulative Hits Incurred vs. Range

Given these initial results, a further investigation was necessary to determine how effective this system was at protecting the ship, not just destroying the missile. This required a simulation dealing with fragment continuation after the missile was destroyed by CIWS. The desired result of this simulation was to determine if any fragments would hit the ship and if so what was the probability. Given the momentum of the missile debris, the size of the ship and the range to the ship, it was assumed that there was a very

large cross section for debris hitting the ship. The simulation took into consideration the fact that fragments vary in size, shape, and masses. Figure (3) represents the data collected for this simulation it can be seen that 70% of the fragments were expected to hit the ship.

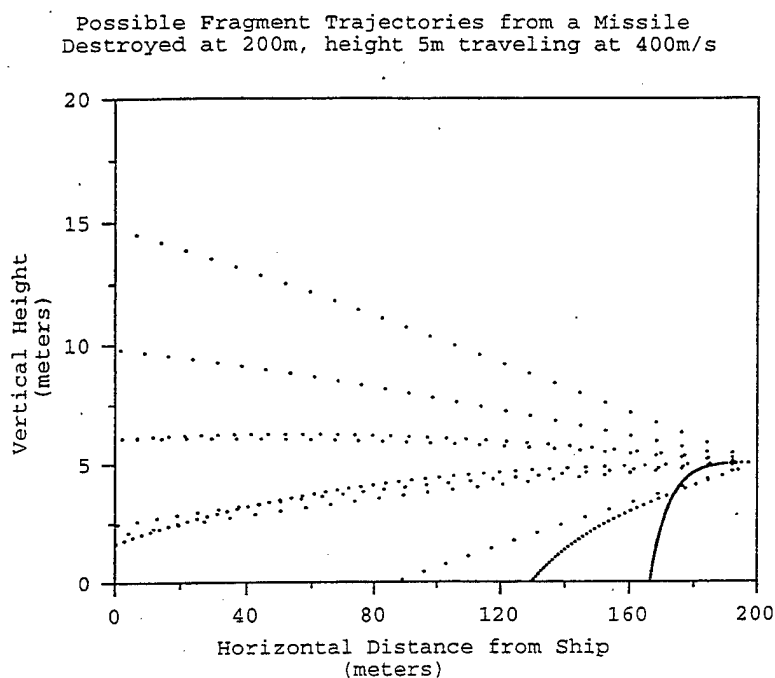


Figure 3. Possible Fragment Trajectories from Inbound Missile

The last and most important part of the CIWS simulations was determining the actual probability of a missile fragment striking the ship. Several thousand random fragments were simulated at ranges from 100-2000m at increments of 100m. The results of this are reproduced for the reader in Figure (4). It can be seen that the closer to the ship that the missile is destroyed, the more likely its fragments are to hit the ship. These

results were expected and it was bad news for those aboard ships. The probability of a fragment striking the ship goes up rapidly as the range decreases. Unfortunately, the results from previous simulations show that the typical destruction range for an incoming missile is 170-190m. For an example, if you assume 200m and 10 fragments then four to five fragments will strike the ship. It was also noted that these fragments were not small chips of paint but rather sizable chunks of metal; the average fragment size was 40 kg, with a final average kinetic energy of 2kJ.

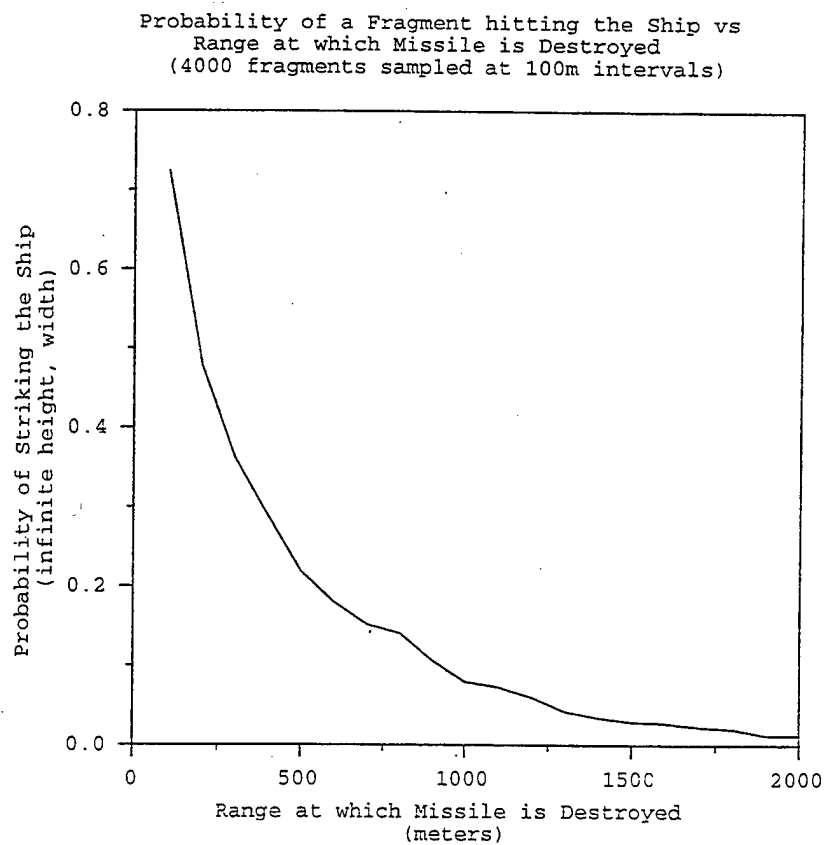


Figure 4. Probability of Fragment Striking Ship vs. Destruction Range

B. ANTI-MISSILE MISSILES

Another kinetic energy strategy being investigated is the antimissile missile. Missile technology is very mature, and the engineering is well developed, so it appears to be a logical approach to kill a missile with a missile. We have been using the theory of long-range detection and engagement with a missile. This method has been a solid solution for a number of years and the military is currently in the process of upgrading their systems. Given a sufficient detection range, the Navy's standard missile is quite capable. Nevertheless, with the improvement of anti-ship missiles there are many inherent problems for the missile-on-missile approach. An example of these inherent problems is the Theater High-Altitude Area Defense (THAAD) program, which to date has not had a successful engagement in tests thus far [3]. The dynamics are proving to be much harder than anticipated. A convenient rule of thumb is that defensive missiles must have three times the maneuverability of the incoming missile [4]. Anti-ship missiles are approaching the ability to fly at speeds over Mach 2, pulling greater than 10g's in terminal maneuvers. Therefore, we are quickly approaching the point where defensive missiles will be required to pull 30g's to adequately counter the maneuver's of the inbound missile. It can be reasonably assumed that shortly after any advances in defensive missile technology are made, the technology will be transferred to offensive missiles. Therefore, the new defensive missile will soon be outdated, and thus ineffective. Additionally, the cost of these missiles also rises as the new technology is employed. This higher cost makes it very expensive to conduct training, given budget limits. Lastly, like the CIWS, a small missile magazine is also a limitation. It is

becoming clear, from the two examples discussed, that kinetic energy weapons cannot provide the protection required in the future.

III. DIRECTED ENERGY WEAPON APPROACH

A. BACKGROUND

Since kinetic energy weapons are not a viable solution for the long term, we must turn to the investigation of the directed energy weapon (DEW). The Department of Defense has shown an interest in DEW since at least the mid-1970s, when it put together its first airborne laser under the program called Airborne Laser Laboratory [5]. Two areas of directed energy weapons are currently being funded by the military: Lasers and High Powered Microwaves (HPM). Whereas kinetic energy weapons have been employed for centuries and are quite well understood, directed energy weapons represent the future and their kill mechanisms are not that well understood. DEWs are normally thought to be soft-kill weapons, though the Mid-Infrared Advanced Chemical Laser (MIRACL) "successfully engaged BQM-34s and supersonic Talos/Vandal missiles in crossing scenarios at tactically meaningful ranges" [6]. The two systems that will be described here have their own merits and pitfalls. Currently, lasers are thought of primarily as defensive weapons whereas the HPM are thought to be more along the line of offensive weapons. However, they share a common improvement over kinetic energy weapons; they strike at the speed of light. This feature is becoming increasingly important as anti-ship missile technology becomes more advanced.

We have seen that CIWS has problems in effectiveness against straight flying missiles and the THAAD program is having problems striking the target. If a defensive weapon can travel at the speed of light, incoming missiles maneuverability becomes a

non-factor and faster response times are achievable. So a closer look at these two emerging technologies is warranted.

B. HIGH POWERED MICROWAVES (HPM)

1. Background

It has been shown that HPM has the potential of being a threat to electronic systems [7]. Additionally, unless a system has been specifically tested and hardened against microwave energy, the system will have essentially no protection. A simple experiment shows the effectiveness of microwaves against electronics. Put a simple operating electronic wristwatch into a home microwave oven. For this thesis, a digital watch was placed in a microwave oven. The watch suffered no noticeable effects after a one-second exposure, but after a three-second exposure, the watch had ceased functioning. There were no visible marks, the watch did not get hot to the touch, but it was inoperable. As the world becomes more reliant on sophisticated electronic weapons, the use of HPM as a weapon appears more enticing.

Microwaves were first artificially generated in the 1880s by Hertz. Since then several advances have been made in the microwave field, including the klystron in the thirties and the magnetron during World War II. The magnetron is probably the best example of a wartime scientific breakthrough that altered the course of a war. The British, under continual air attack from Germany, were in need of a system that would provide early warning that an attack was eminent, thereby allow them to prepare. The solution to their problem was the invention of radar. The magnetron, a microwave source, was the essential element of the radar system. It was a wartime development so

its deployment was faster than it would have normally been. As with most new technologies that are very different from the norm, it takes time before it is universally accepted. Today radar is an invaluable tool that has been integrated into the heart of warfare.

Recently the sources for HPM have taken large strides forward, in being able to provide large relativistic electron beams in excess of a gigawatt and with the miniaturization of the sources. So in the 1980s, HPM weapons received another look and the field has enjoyed a renewed vigor [8]. Microwave technology itself is very mature, although coupling it with today's sources is new evolving field. Figure (5), taken from "An Introduction to High Power Microwaves" by James Benford, depicts the emergence of HPM as a historical trend.

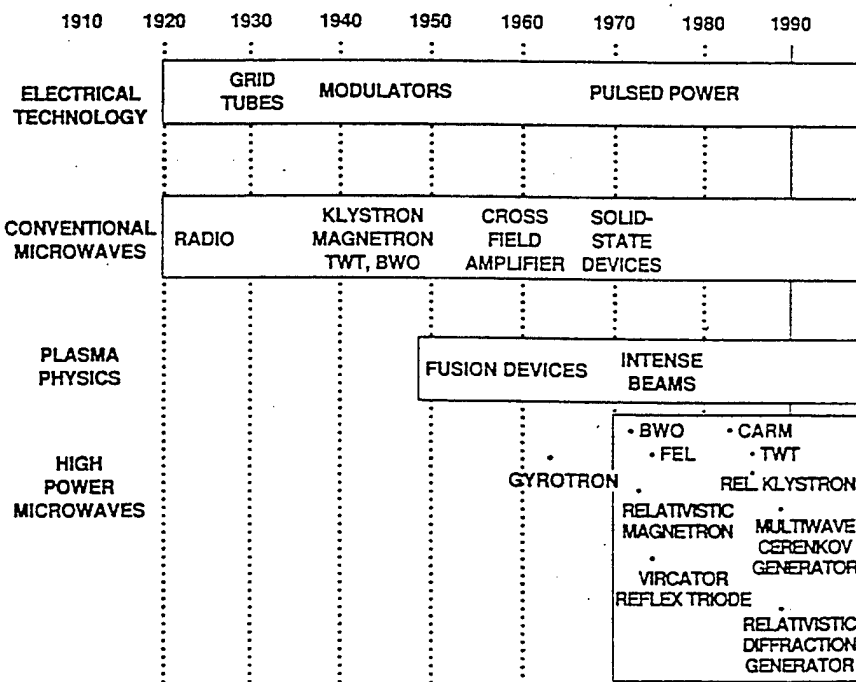


Figure 5. The history of high-power microwaves

When talking about the use of high power microwaves as a weapon, it is convenient to talk in terms of power density. The power density on the target from a microwave signal transmitted from a fixed-size antenna is proportional to a quality factor, pf^2 . This can be derived from relating the power density on the target with the energy flux on the target using the diffraction limit. Figure (6), taken from "An Introduction to High Power Microwaves" by James Benford, shows the general history of the development of microwaves in terms of pf^2 .

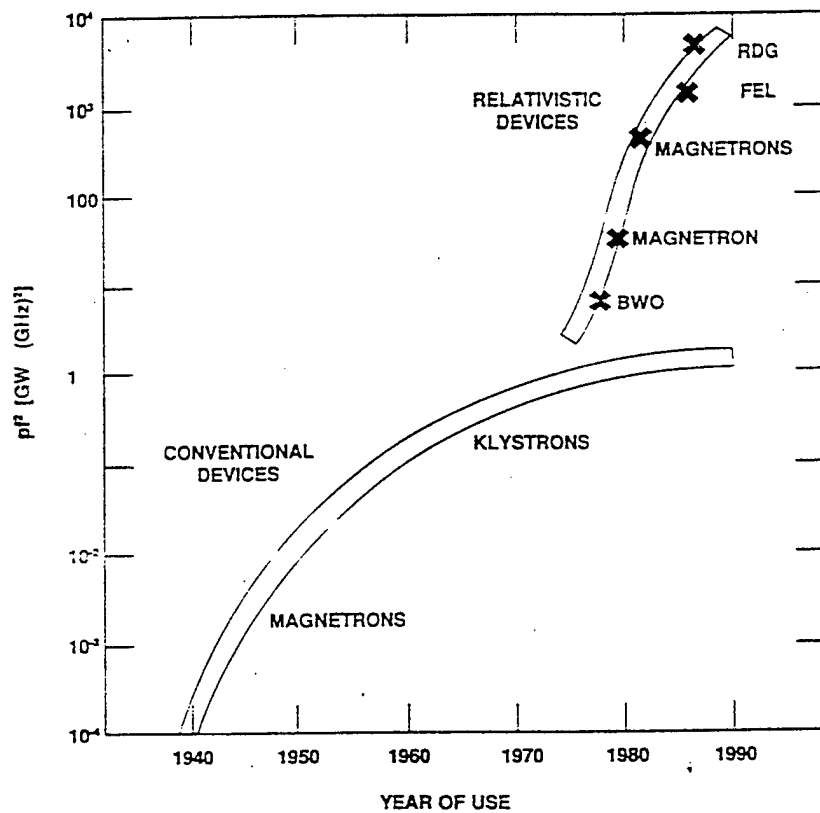


Figure 6. The growth of microwave devices in terms of quality factor pf^2
 Two types of attack modes against electronics have been proposed. In one, an HPM fires an intense pulse to disable a specific target at substantial range. In the second

HPM attack mode, large areas are swept with a radiating pulse in hopes of disabling a significant number of targets [9]. Since the second mode of attack has debatable effectiveness against military targets, we will concentrate on the first mode of attack, which is more suitable for military applications.

2. Source Selection

It can be seen from the quality factor, pf^2 , that if we want to maximize the power density on the target then we must start with a viable source. Such a source would provide an output power that exceeded 1 GW. Figure (7), taken from *High-Power Microwave Systems and Effects* by Clayborne Taylor, is a comparison of peak power and frequency of current sources. Figure (7) also depicts the range of frequencies that in combination with power density requirements delineate the currently available HPM sources. Due to propagation concerns, available microwave sources, and initial effectiveness testing the effective frequency range for a HPM weapon is 500 MHz to 12 GHz. Ideally, it would fall between 500 MHz and 3 GHz. In addition to output power and frequency range requirements, a source should be stable in frequency (<1% bandwidth) with an efficiency of about 30% [10].

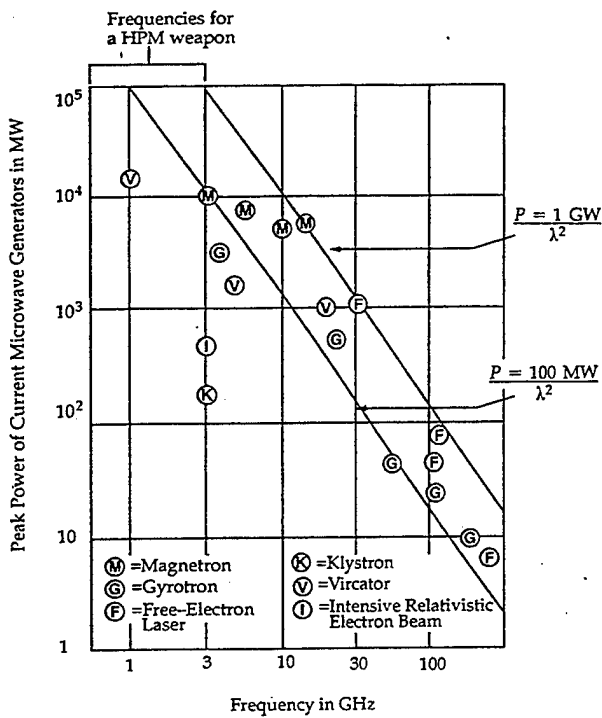


Figure (7) peak power comparisons

3. Propagation

It is useful to determine the amount of power that can be delivered at a distance for a given source and antenna. The power radiated, P_r , is dependent upon the power from the source, P_s , the directivity of the antenna, G_D , and the efficiency of the antenna, ϵ . Directivity is the measure of an antenna's ability to concentrate radiated power in a particular direction. It can be expressed as the ratio of the beam area, Ω_A , and the 4π steradians of all the solid angles:

$$G_D = \frac{4\pi}{\Omega_A} \quad (\text{III.B.1})$$

Therefore

$$P_r = \varepsilon P_S G_D = P_S G, \quad (\text{III.B.2})$$

where $G = \varepsilon G_D$ is the gain of the antenna. Ω_A is the beam area or "spot size" and is equal to $(\pi/4)(\Delta\theta)^2$ where $\Delta\theta = 1.22 \lambda/D$ is the half angle of the first minimum in the diffraction pattern of a circular antenna. One finds

$$G = \frac{4\pi A \varepsilon}{\lambda^2} \quad (\text{III.B.3})$$

where A is the antenna area, D is the diameter of the aperture, λ is the transmitted frequency and ε is the antenna efficiency.

If the range to the target is in the far-field region, then the intensity drops off proportional to $1/R^2$, where R is the range to the target [12]. The far-field distance is $R_{ff} = 2D^2/\lambda$. Using an antenna diameter of $D = 1\text{-}10 \text{ m}$ and a transmitted frequency of 1-3 GHz, the far-field distance is not greater than 2 km. Since, the goal is to engage an inbound missile from 5-10 km, we can assume we are in the far-field. Therefore, neglecting atmospheric effects we have the power density at the target:

$$P/A_B = \frac{GP_S}{4\pi R^2} \quad (\text{III.B.4})$$

where A_B is the spot size of the beam.

Another simple method for calculating power density at the target is to use nomographs. Figure (8) is a nomograph that provides a method for determining relevant HPM weapon parameters [13]. Since the nomograph does not account for attenuation losses and assumes a 100% efficient parabolic antenna, only ideal values are obtained. The nomograph can be used in two ways: 1) assume a required power density and find

the required technology and equipment 2) given physical and technological constraints, find the maximum power density for a given range.

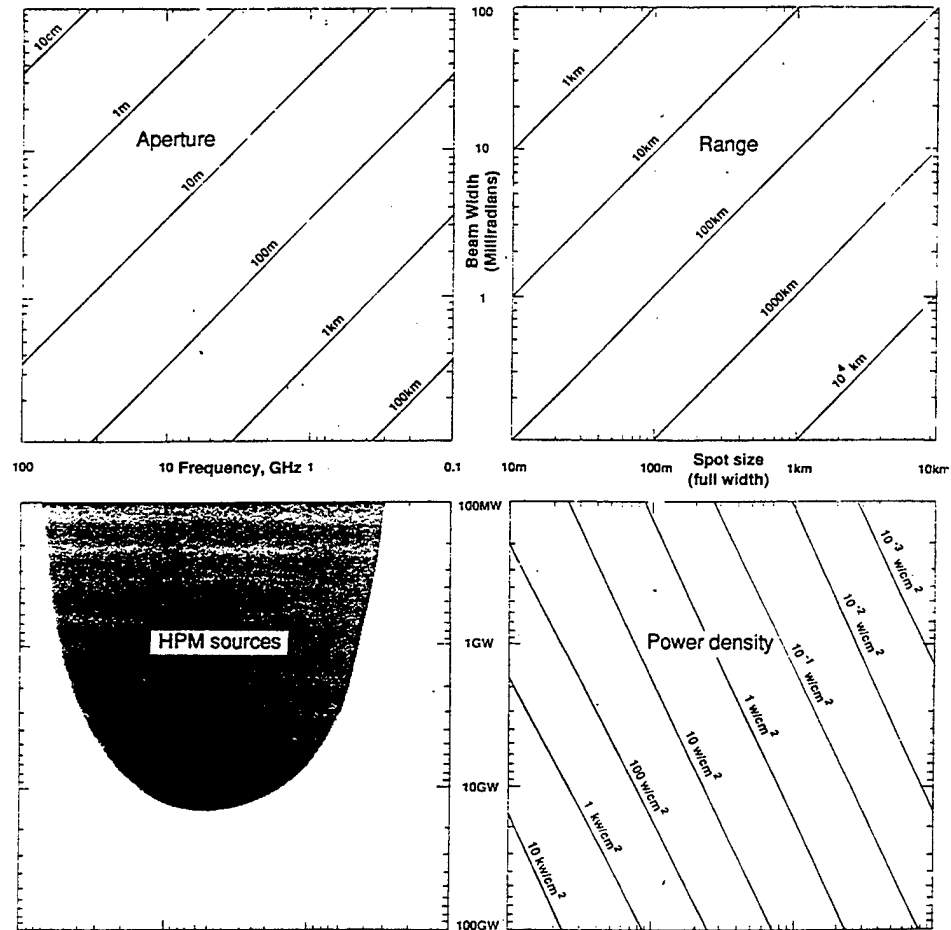


Figure 8. HPM parameter nomograph.

The use of the nomograph is explained by the following example. Choose a frequency of 5 GHz and a radiated power of 10 GW by placing a point at the intersection of the two values in the HPM sources quadrant. Next, choose an antenna diameter of

10 m, by drawing a vertical line from the first point to the intersection of the 10 m line in the Aperture quadrant. By drawing a horizontal line from this point, we find a beam width of roughly 8.3 mrad. Next, choose a range of 10 km, by continuing the horizontal line until it crosses the 10 km line in the Range quadrant. The final step is to draw a horizontal line from the first point to the Power Density quadrant and then draw an intersecting vertical line from the Range quadrant. The result is a power density of 100 W/cm² and a full width spot size of 80 m [13].

As microwave energy propagates through the atmosphere, it is attenuated by the water gas molecules present in the air. Figure (9), taken from *High-Power Microwave Systems and Effects* by Taylor and Giri, and Figure (10), from *High Power Microwaves* by James Benford, provide representative attenuation factors.

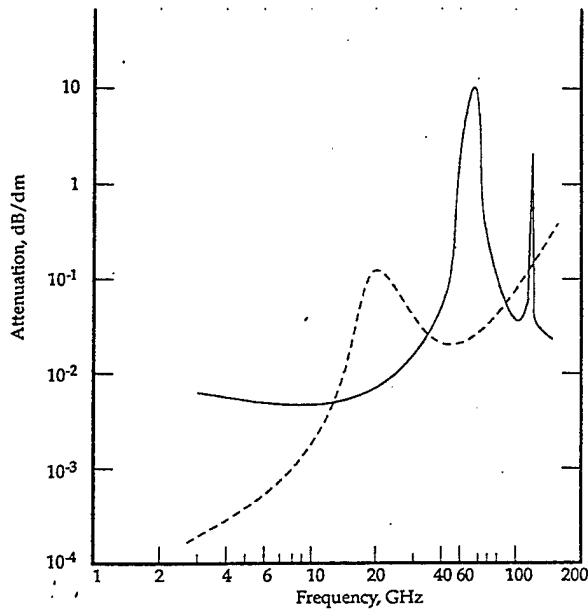


Figure 9

Figure 9 & 10. Attenuation due atmospheric attenuation

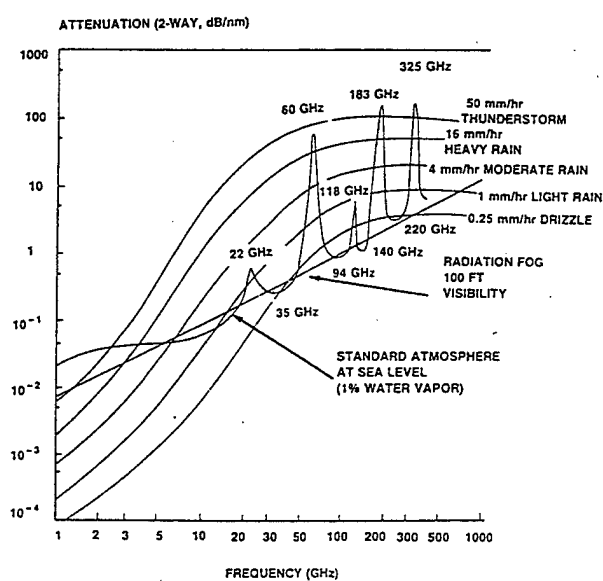


Figure 10

These Figures show that at the lower microwave frequencies attenuation due to oxygen and water vapor absorption is very small. However, at higher frequencies attenuation becomes a significant problem. Accounting for signal attenuation, α , provided by Figure (9) we arrive at the atmospheric corrected power density on the target:

$$P / A_B = \frac{GP_S}{4\pi R^2} e^{-\alpha R}. \quad (\text{III.B.5})$$

Spherical spreading of the emitted energy can be an advantage or disadvantage depending on the intended mission. If the mission is to saturate a large area with microwave power, then the spreading will be an advantage. On the other hand, if multiple ships are operating in unison it might prove impossible to employ HPM for fear of irradiating another ship, due to the large beam size.

Regardless of the mission, there are some inherent problems, "suicide" and "fratricide", that must be dealt with. These problems result from using an antenna-directed weapon, side lobes and strong local fields [13]. Fratricide is unintended damage to nearby electronics or personnel due to side-lobe emissions from the weapon. In the "fog of war," the potential for damage to friendly forces near at hand could be a serious limitation. The problem may be somewhat mitigated by side lobe suppression, which would have to be fully investigated and understood. The second problem, suicide, is unintended damage to the subsystems of the HPM platform itself due to its own emitted pulse. This problem may be solved by shielding, but the weight and size of the extra shielding will be topside and must be accounted for when comparing systems [14].

4. Effects

In many studies and experiments, it has been shown that intense microwave radiation can have serious effects on today's electronics. Once microwave energy reaches a target, a sequence of penetration and propagation processes will take place from the outer surface into the electronics. The energy arrival can be via "front-door" or "back-door" paths. A front-door path is a path that is designed for microwave transmission. An example is a receiving dish that is connected to an electronic box via coaxial cable. A back-door path is an inadvertent point of entry (POE) for electromagnetic energy penetration, such as access doors, cracks, seams, connectors and cable shields [15].

Possible modes of electronic disruption are called intermodulation, latch-up, thermal damage, punch-through or digital upset, as described below. A more detailed description is available in *High-Power Microwave Systems and Effects*, by Taylor and Giri.

Digital Upset: Digital circuits generally use CMOS or bipolar transistor technology and are vulnerable to HPM coupling damage. Damage can be temporary, as in the change of the stored or transmitted information due to indirect coupling. It may also be permanent when the HPM illumination is directed directly onto the chip package [16].

Intermodulation: Intermodulation is associated with electromagnetic interference and it stems from operating multiple sources with non-linear elements simultaneously. These elements can be located in the target's transmitters, response circuits or the propagation path [16].

Punch-Through: Punch through is a when there is an increase in biasing voltage, which causes the depletion region to expand in a reverse biased *pn* junction. If the depletion region expands into another junction, then the high current may damage the junction [16].

Latch-Up: Latch-up is the condition when a semiconductor device no longer responds to input signals. Latch-up generally occurs when an inadvertent multi-junction is formed, which triggered disables the device. Latch-up can result from several sources including: photoelectric generation from ionizing radiation; thermal heating causing impact generation and when minority carriers are injected into the substrate by a transient forward bias on parasitic *pn* junction [16].

Figure (11) is a plot of damage thresholds vs. sample components, the interaction of microwave energy with these individual components becomes very complicated when the entire system is evaluated. Due to the manner in which induced microwave energy must propagate, first through the external shielding, then the outer surface material and then the external cavities, to penetrate into the interior of the system. The energy must then interact with the internal wiring, internal cavities, and possibly internal shielding. Then finally, the residual energy must interact, with a vital component such as those listed in Figure (11). This final interaction may cause permanent or temporary damage, depending on the residual energy level and the damage threshold of the electronics. The kill mechanism and probability of kill (pk) for any given target will be need to be assessed individually. The resultant damage is hard to predict without extensive testing of every piece of electronics targeted. Though many studies have been conducted on

small simple electronic devices, to compile the necessary database of effects on complex military hardware would be very costly.

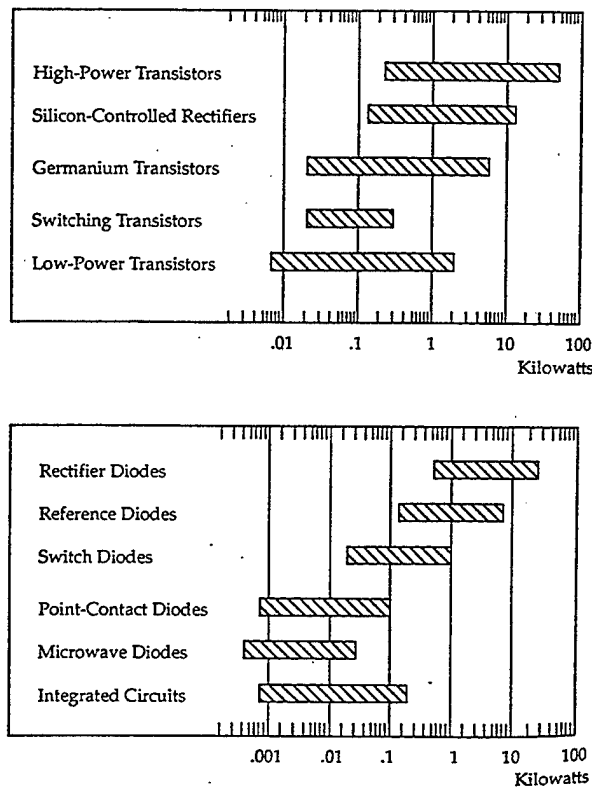


Figure 11. Damage threshold power ranges for representative components

5. Hardening

Until recently, the use of HPM as a weapon has not been a threat. Therefore, there is a dearth of information concerning the shielding of HPM. However, there have been many studies done on EMP hardening, since we have lived with the threat of nuclear blasts for many decades. Despite the fact that the majority of the testing was not done at HPM frequencies, and therefore cannot be applied to HPM shielding, some

results remain valid. In theory, a Faraday shield, a simple metal enclosure, is an effective shield against microwave energy.

The effectiveness of a Faraday shield can be simply demonstrated at home again with a digital watch and a microwave oven. Using the same model microwave oven and watch that were used to demonstrate the effectiveness of microwaves against electronics but now add a piece of aluminum foil. A second series of home experiments were done for this thesis. The watch was inserted into a small box constructed of aluminum foil. The foil box was then placed in the microwave and the oven was subsequently turned on. This process was repeated several times turning on the microwave oven for various time periods ranging from 1-90 seconds, checking the watch's after each exposure. The watch suffered no noticeable effects.

Figure (12), taken from *Principles and Techniques of Radiation Hardening* by Norman Rudie, shows the shielding effectiveness for various meshes and woven screens. A woven screen of 0.002" copper has a shielding effectiveness of approximately 60dB at 1 GHz. This provides a very effective shield against typical HPM frequencies.

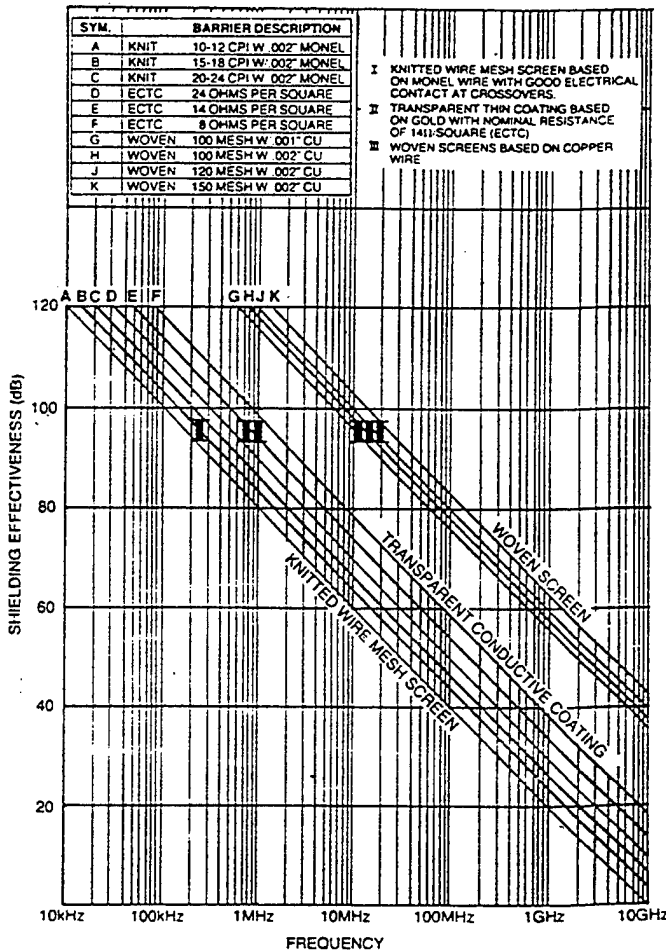


Figure 12. Barrier Shielding Performance for shielding windows [17]

In addition to Faraday shielding, there are other methods to harden a system to microwave energy. They include the use of low pass filters, diode limiters, feed-through capacitors, and the filling of any empty voids with filler material. Therefore it appears that a hardening technique could be effective applied against incident microwave energy. If the shielding is not maintained vigorously, its effectiveness will decrease rapidly. This

makes shielding a room or a building exceedingly difficult, due to the human traffic. However, this would not be the case for an anti-ship missile, as they are rarely opened.

6. Conclusion

Due to their relatively large carrying capacity and available power, ships may be the first to deploy a HPM weapon. However, the issues of the spreading energy and shielding should be first resolved. It might be possible for tactics to be written that would enable a ship to defend itself without inadvertently impairing another ship. In addition, shielding against HPM may end up being an expensively prohibitive process. If so, these costs may counter the high cost of developing and deploying the HPM weapon.

C. LASERS

1. Background

The second DEW approach involves lasers. The ideal weapon is one that always hits its target with sufficient energy to neutralize the target. Further, it should be able to instantaneously hit any target in sight, no matter how far away it is. High-energy lasers are closer to ideal than any other weapon in that they shoot a precise beam of energy, which travels at the speed of light and only takes about 30 microseconds to travel 10 km[18].

Laser weapons have been a fantasy weapon for several decades. Nevertheless, their reality was proven by the Air Force's ALL project of the late 1970s, and the Navy's MIRACL project of the 1980s. While these two projects had many early successes that seemed to hold the promise of a laser weapon on the horizon, they also illustrated the vulnerabilities of lasers. The Strategic Defense Initiative (SDI) was another project of the

1980s. It was designed to provide the US with an "umbrella" capable of destroying incoming nuclear missiles, therefore rendering nuclear weapons as strategic weapons obsolete. However, the high cost of development, the collapse of the Soviet Union, and the overly optimistic predictions caused the SDI program to be halted. Consequently laser weapon research was neglected for many years, but the Air Force has revived it with its chemical oxygen iodine laser (COIL) project. The Air Force is currently working very earnestly in solving the problems associated with laser weapons. The problems associated with lasers are their high cost, tracking requirements, weight, size, and atmospheric propagation problems.

Due to the inherently short wavelengths of the lasers, a dish much smaller than that required for the use with HPM could be employed. Therefore, very little of the precious topside real estate would be used. This concept has been previously covered [19]. The optics and requisite tracking system already exist to make this a weapon, though the system would require further engineering for deployment. As stated previously the chemical laser MIRACL has already successfully engaged missiles in flight at long range.

Though MIRACL was a successful platform for testing the basic theory of laser effectiveness, it had a few shortcomings for being a deployable shipboard system. MIRACL is a chemical laser using Deuterium Flouride. Chemicals would need to be carried on board the ship, which would mean more space required and a somewhat limited magazine. The waste gases produced by the laser are also toxic, representing a personnel hazard and a storage problem. Lastly, the wavelength of $3.8\mu\text{m}$, which was

chosen to exploit an atmospheric propagation window, has proven to be inadequate because of thermal blooming. Since MIRACL is a chemical laser, its wavelength and vulnerability to thermal blooming cannot be changed.

An FEL may be able to correct these shortcomings. An FEL can be powered by a modified shipboard distribution system, giving it an almost unlimited magazine [20]. Additionally, due to the tunability of the FEL, the problem of atmospheric absorption may be overcome with the selection of a different wavelength laser beam. The FEL also has hazards and limitations. An operating FEL produces nuclear radiation and requires an electron beam dump, but these problems have been addressed [21]. Although, there is no theoretical reason for an FEL not to be able to produce several megawatts of power the current world record of only 340 W average power is held by Thomas Jefferson National Accelerator Facility, TJNAF [22]. There are plans to raise that to 20 kW within the next few years.

2. Atmospheric Propagation

One of the most important aspects of the laser weapon is the understanding the laser propagation through the air. This section primarily focuses on the propagation of laser energy and thermal blooming, possibly the biggest hurdle for the realization of a laser weapon.

We begin without atmospheric effects. Start with a definition of energy flux, Φ , or power density as the ratio of the power, P , to the spot size, A . We can mathematically express Φ as

$$\Phi = \frac{P}{A} = \frac{P}{\pi(R\theta)^2}, \quad (\text{III.C.2.1})$$

R is the range and θ is the beam half angle in the far field. Additionally the energy fluence, F , is the amount of energy deposited on a target in a given time. To find F , we can integrate Φ with respect to time, t :

$$F = \int \Phi dt = \Phi \tau, \quad (\text{III.C.2.2})$$

where τ is the pulse length and Φ is constant. We can get an expression for F by substituting Eq. (III.C.2.1) and $\theta = 1.22\lambda/D$, for a diffraction limited beam, into Eq. (III.C.2.2) where D is the diameter of the aperture and λ is the wavelength of light. Therefore, for propagation in the far-field in a vacuum we get:

$$F = 0.21 \frac{PD^2\tau}{(\lambda R)^2}. \quad (\text{III.C.2.3}).$$

Since fluence is a measure of how much energy is absorbed, it can also be related to target hardness. The greater the fluence threshold is, the harder it is for the laser to do damage.

In reality, the laser energy is not traveling through a vacuum, but rather through the atmosphere where there is attenuation. Figure (13) shows various atmospheric transmittance values for 0-15 μm wavelengths, over a 1820-meter horizontal path at sea level. Figure (13) illustrates the importance of wavelength selection for laser weapon use. In a vacuum, we have 100% transmission, but Figure (13) shows a transmission range of 0-90% depending on wavelength. The difference is due to atmospheric attenuation. There are two main attenuation mechanisms associated with propagating through the atmosphere they are; scattering and absorption. Scattering is the re-direction of energy due to collisions with aerosols and other particles entrained in the air. If the

energy is deflected by a sufficient amount, it will not reach the target. The second attenuation mechanism, and ultimately more limiting, as we will find out later, is absorption. It is caused by the loss of energy to the atmosphere, due to molecular absorption.

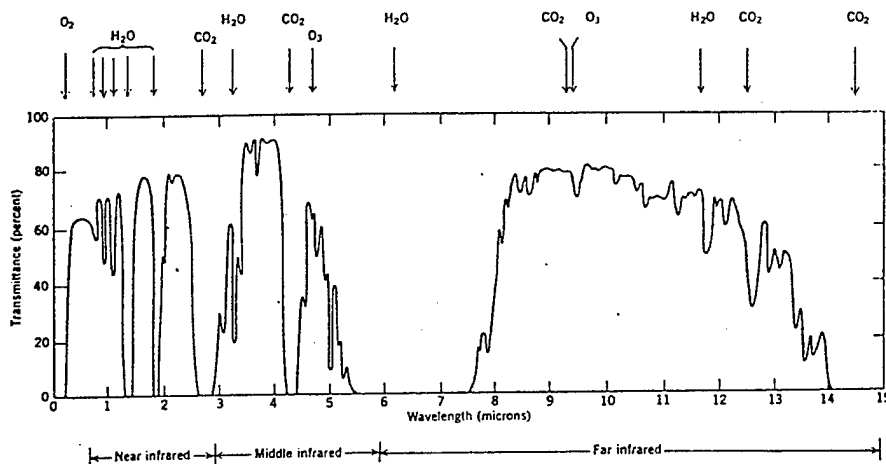


Figure 13. Atmospheric Transmittance for 0-15 μm

Figure (13) is a good basic plot of transmittance, but a more useful plot would separate the effects of scattering and absorption. Figure (14) gives representative attenuation coefficients for scattering and absorption and it shows the combination of the two as an extinction coefficient. The rural conditions of Figure (14) are conditions that MIRACL might typically encounter. However, we are more concerned with maritime conditions and they are generally different from rural conditions due to an increase in air moisture. Therefore, the two different atmospheric conditions have different attenuation coefficient values. Figure (15) shows the maritime attenuation coefficients for the same range of wavelengths. Notice that while the maritime extinction coefficients are

generally the same, the absorption and scattering coefficients differ vastly at some wavelengths. It is important that the atmospheric conditions for which the laser will operate be taken into consideration.

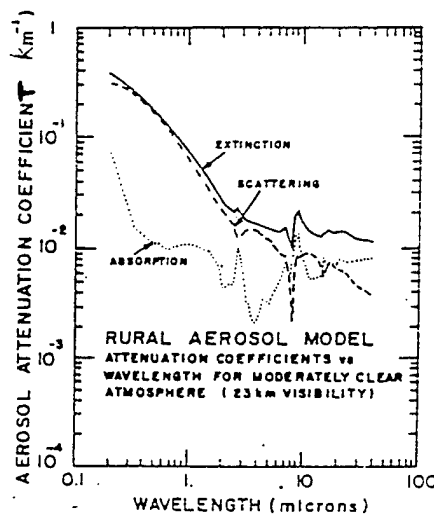


Figure 14

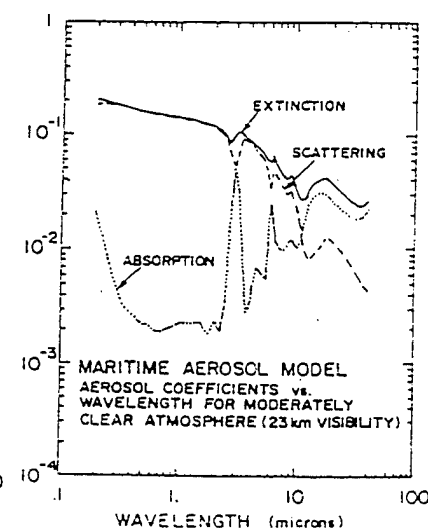


Figure 15

Figure 14 & 15. Atmospheric attenuation coefficients

Looking at Figures (14) and (15), it would appear that scattering would be more limiting at shorter wavelengths. While it is true that the attenuation coefficient for scattering is larger than that for absorption, absorption leads to thermal blooming because the local heating of air lowers the index of refraction. These small changes in refraction affect the propagating light beam as if the light beam were traveling through a lens. The beam may change direction "beam wander" or the intensity of the beam might fluctuate, "scintillation". We observe these effects in everyday life. These small changes in local indexes of refraction cause the twinkling of the stars and the shimmering of distant objects on a hot day. In general, these effects are linear and a laser weapon can overcome

them with an increase in power or use of a fast tracking optical system. However, in certain cases, such as still air and for sufficiently high laser energy, a strong effective divergent lens is formed in the air, causing the laser energy to be dispersed. Only a fraction of the dispersed energy would reach the target. This effect is known as "thermal blooming", and it is non-linear in nature. Increasing power levels only speeds the onset of thermal blooming. Thermal blooming is most serious for head-on shots, due to the still air. We need to find a wavelength that minimizes absorption.

Since lasers are capable of producing narrow laser lines we need a more detailed plot of atmospheric transmission than supplied by Figure (13). If we used Figure (13) we might miss a window or chose a wavelength such that there would be very little transmission. Figure (16), taken from Rudie [23], shows a more detailed plot of representative transmission that might be used vice Figure (13). Additionally, we need to remember that absorption is more important than scattering, due to the possibility of thermal blooming.

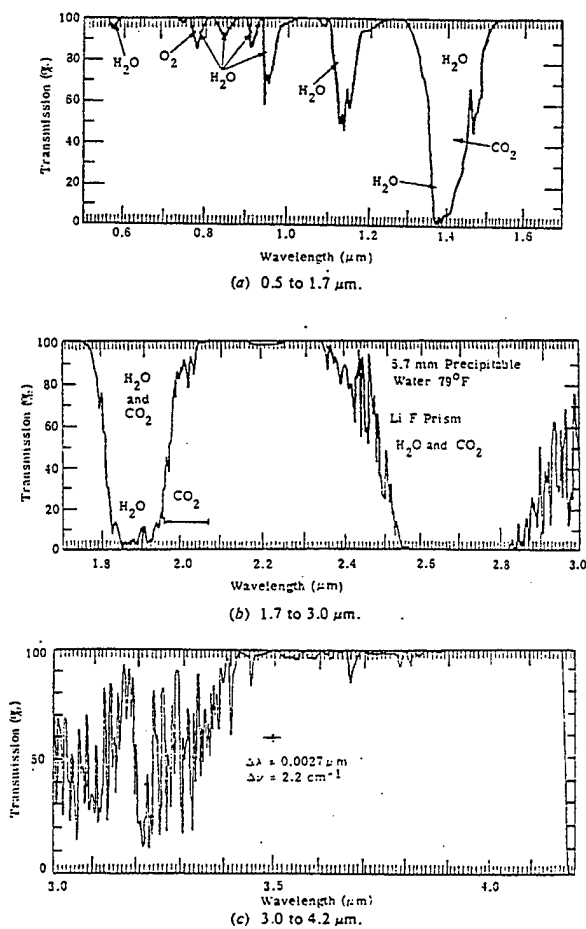


Figure 16(a-c). Atmospheric Transmission

Different types of lasers produce different wavelengths and different light spectra.

Figure (17) shows the laser output of two chemical lasers. The MIRACL is a nominal $3.8 \mu\text{m}$ laser, but it actually has many laser lines. If we use the atmospheric transmission plot for only $3.8 \mu\text{m}$, some of the other laser lines may cause thermal blooming. What is needed is a laser that is capable of putting out a single narrow line. For ship defense, the FEL would be the preferred choice and could be designed to the desired wavelength, thus delaying or avoiding the onset of thermal blooming.

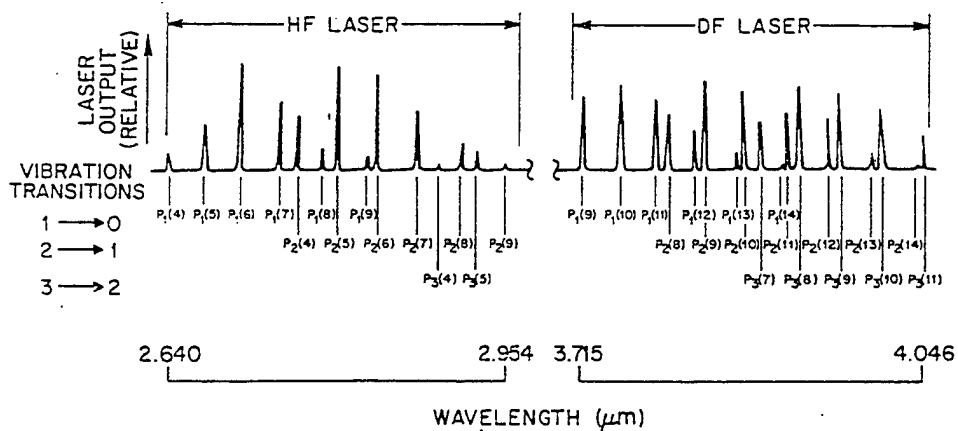


Figure 17. HF and DF laser output

In 1997, Cook and Albertine published a paper on the atmospheric propagation issues related to a maritime deployed high-energy laser weapon system (HELWS) [24]. Figure (18) shows a comparison of absorption coefficients, computer simulated, for the different wavelengths selected. The most promising wavelength from this plot is 1.042 μm , with the YAG laser line of 1.06 μm as a close second. Both of these laser lines show significant improvement over the MIRACL laser line of 3.8 μm for maritime conditions.

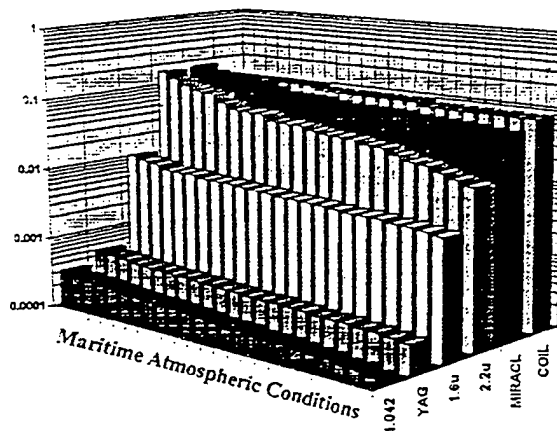


Figure 18. Total Absorption 1/km [24]

Figure (19) shows the total extinction coefficients, computer simulated, for the same wavelengths. It is apparent from Figure (19) that while absorption coefficients of the shorter wavelengths are a couple of magnitudes better than those of the longer wavelengths, their extinction coefficients suffer by a factor of 2-3 for extreme weather conditions. The study concluded that the $1.6 \mu\text{m}$ laser line was the best choice due to eye safety concerns. Its performance variation was the smallest under different atmospheric conditions. If it is possible to prevent thermal blooming at this range, then the added benefit of eye safety would warrant the use of this wavelength. However, it appears that the shorter wavelengths of $1.042 \mu\text{m}$ and $1.06 \mu\text{m}$ are preferred.

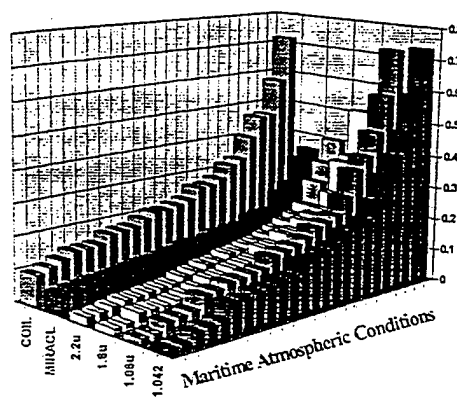


Figure 19. Total extinction 1/km [24]

3. Conclusion

In conclusion, laser weapons have a proven capability to be viable defense weapon in the future. However, for lasers to become deployable, they must address the many atmospheric conditions that affect a laser beam during its propagation from the ship

to the target. The most threatening effect is thermal blooming, as the onset of thermal blooming prevents the laser energy from reaching the inbound missile. Tactics that would have two ships working together, each providing air defense for the other, in order to avoid propagating the laser beam through stagnant air conditions. Since this would limit the ship flexibility, it would be preferable to find another solution.

While choosing a shorter wavelength of light can reduce the amount of energy absorbed by the atmosphere, these shorter wavelengths are more susceptible to extinction due to adverse weather conditions. To make the laser a robust weapon system, the problem of adverse weather must be solved. Current studies are determining the losses of laser energy in rain and fog for power beaming energy to space stations [25].

IV. FEL THEORY

A. BASIC OPERATION

A free electron laser (FEL) uses a source of electrons typically from an electron gun, that are injected into an accelerator where they reach relativistic energy, γmc^2 , where γ is the Lorentz factor, m is the electron rest mass and c is the velocity of light. In addition to being accelerated, the electrons also exit the accelerator in a stream of microbunches, which were formed due to the dynamics of the accelerator. These microbunches of relativistic electrons are the input into the undulator, which is the heart of the FEL.

Within the undulator, the optical field is amplified by the interaction of the relativistic electron beam, the optical wave, and the spatially periodic magnetic field produced by the magnets of the undulator. The length of the undulator, L , is equal to the product of number of undulator periods, N , and the undulator wavelength, λ_o , as shown in Figure (20). The spatially periodic magnetic field, represented by the up and down arrows, can be from electromagnets, but is usually constructed with permanent magnets. Figure (20) also depicts the mirrors of an optical resonator, which is needed for FEL oscillator. The mirrors forming the resonator contain the optical field while it interacts with the electron beam. The mirror at the far end of the undulator is partially transmitting or has a hole in it to allow a small percentage, typically 1-10%, of the optical field power to leave the resonator and to be used as laser light.

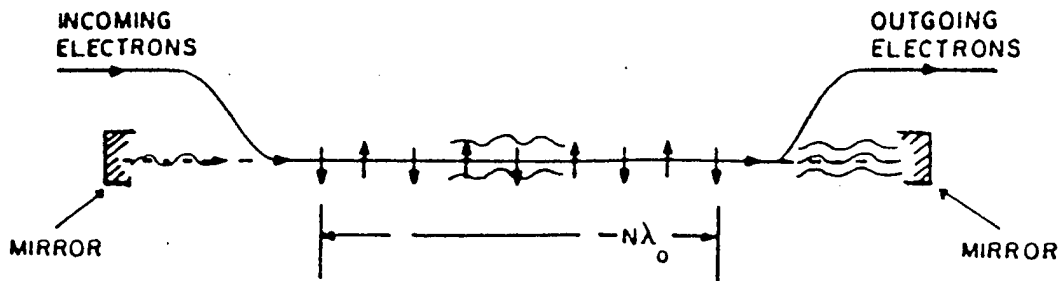


Figure (20). Basic undulator and resonator configuration.

The amplification of laser light from the resonator is dependent upon the interaction of the electron beam, the optical wave, and the magnetic field of the undulator. The electron bunches that are emitted from the accelerator, are traveling at a speed of $\beta_z c$, where β_z is the axial component of the velocity and c is the speed of light. As the electron bunches traverse the length of the undulator, they are accelerated by the magnets of the undulator in the transverse direction. In order for the electrons to interact strongly with the optical field, they must satisfy the resonance condition one wavelength of light, λ , passes over an electron as the electron travels a distance of one undulator wavelength, λ_0 [26]. The resonance condition relating the electron energy, λ , and λ_0 can also be expressed as:

$$\lambda = \frac{(1 + K^2) \lambda_0}{2\gamma^2},$$

where $K = eB\lambda_0/2\pi mc^2$ is the undulator parameter that will be derived in the next section and γ is the relativistic Lorentz factor.

B. PENDULUM EQUATION

The energy transfer to the optical beam from the electron beam occurs in the undulator section. Assuming that we are analyzing a helically polarized undulator, then the magnetic field can be represented as

$$\vec{B}_u = (B_x, B_y, B_z) = B(\cos(k_o z), \sin(k_o z), 0), \quad (\text{IV.B.1})$$

where $k_o = 2\pi/\lambda_o$ and z is along the undulator axis. The electrical and magnetic field of the optical wave, can be represented by

$$\vec{E}_r = E(\cos(\Psi), \sin(\Psi), 0), \quad (\text{IV.B.2})$$

$$\vec{B}_r = B(\sin(\Psi), \cos(\Psi), 0), \quad (\text{IV.B.3})$$

where $\Psi = kz - \omega t + \phi$; $k = 2\pi/\lambda$; ω being the radial frequency, k being the wave number and ϕ being the optical phase angle.

To be able to describe electron motion, we must determine what significant forces are present in the undulators that affect the motion of an electron. We start with the relativistic Lorentz force equations,

$$\frac{\partial(\gamma\vec{\beta})}{\partial t} = -\frac{e}{mc} [\vec{E}_r + \vec{\beta} \times (\vec{B}_r + \vec{B}_u)], \quad (\text{IV.B.4})$$

$$\frac{\partial\gamma}{\partial t} = -\frac{e}{mc} \vec{\beta} \cdot \vec{E}_r, \quad (\text{IV.B.5})$$

$$\gamma^{-2} = 1 - \vec{\beta}^2. \quad (\text{IV.B.6})$$

If you substitute the undulator and the optical fields into the Lorentz force equations, you get the following

$$\frac{\partial(\gamma\bar{\beta}_\perp)}{\partial t} = -\frac{e}{mc} [E(1 - \beta_z)(\cos(\Psi), -\sin(\Psi), 0) + B\beta_z(-\sin(k_o z), \cos(k_o z), 0)], \quad (\text{IV.B.7})$$

$$\frac{\partial(\gamma\bar{\beta}_z)}{\partial t} = -\frac{e}{mc} [E(\beta_x \cos(\Psi) - \beta_y \sin(\Psi)) + B(\beta_x \sin(k_o z), \beta_y \cos(k_o z))]. \quad (\text{IV.B.8})$$

$$\frac{\partial\gamma}{\partial t} = -\frac{e}{mc} E[\beta_x \cos(\Psi) - \beta_y \sin(\Psi)]. \quad (\text{IV.B.9})$$

For a relativistic electron $E(1 - \beta_z) = E/2\gamma^2$, which is negligible compared to $\beta_z B$ for $\gamma \gg 1$.

We can ignore the E term in the first equation and only include the transverse force of the undulator, which gives us

$$\frac{\partial(\gamma\bar{\beta}_\perp)}{\partial t} = -\frac{e}{mc} B\beta_z(-\sin(k_o z), \cos(k_o z), 0), \quad (\text{IV.B.10})$$

which we can now integrate this with respect to t to find that

$$\bar{\beta}_\perp = -\frac{K}{\gamma}(\cos(k_o z), \sin(k_o z), 0). \quad (\text{IV.B.11})$$

The transverse motion of the electron is very small since $\beta_\perp = K/\gamma \ll 1$ for $\gamma \gg 1$. Insert

$\bar{\beta}_\perp$ into the equation for $\partial\gamma/\partial t$ to find that

$$\frac{\partial\gamma}{\partial t} = \frac{eEK}{\gamma mc} \cos(\zeta + \phi), \quad (\text{IV.B.12})$$

where the electron phase is $\zeta = (k + k_o)z - \omega t$. The initial value for the electron phase is

$\zeta(0) = \zeta_o = (k + k_o)z_o$ at $t = 0$. For relativistic electrons $k \gg k_o$ so that $\zeta_o \approx kz_o = 2\pi z_o/\lambda$.

The electron phase, ζ , determines the z position relative to an optical wavelength, λ .

Now we use $\bar{\beta}_\perp$ in the third Lorentz force equation to solve for γ .

$$\gamma^{-2} = 1 - \bar{\beta} \cdot \bar{\beta} = 1 - \beta_z^2 - \beta_\perp^2 = 1 - \beta_z^2 - K^2/\gamma^2, \text{ or } (1 + K^2)\gamma^{-2} = 1 - \beta_z^2,$$

where $K = eB\lambda_o/2\pi mc^2$ is called the undulator parameter. If we now take the time derivative to relate $d\gamma/dt$ and $d\beta/dt$

$$\frac{\dot{\gamma}}{\gamma} = \frac{\gamma^2 \beta_z \dot{\beta}_z}{(1 + K^2)}. \quad (\text{IV.B.13})$$

Taking the first derivative of the electron phase, ζ , with respect to time, we get

$$\dot{\zeta} = (k + k_o)c\beta_z - \omega, \quad (\text{IV.B.13a})$$

then the second derivative of ζ is

$$\ddot{\zeta} = (k + k_o)c\dot{\beta}_z. \quad (\text{IV.B.14})$$

Solving Eq. (IV.B.14) for $\dot{\beta}_z$ and then substituting into Eq. (IV.B.13) gives us

$$\frac{\dot{\gamma}}{\gamma} = \frac{\gamma^2 \beta_z \ddot{\zeta}}{(1 + K^2)(k + k_o)c}, \quad (\text{IV.B.15})$$

for relativistic electrons $\beta_z \approx 1$, $k \gg k_o$, and

$$\frac{\dot{\gamma}}{\gamma} = \frac{\ddot{\zeta}}{2\omega_o} \quad (\text{IV.B.16})$$

where $\omega_o = \omega(1 + K^2)/2\gamma^2$, $\omega_o = k_o c$, $\omega = kc$ and If we then solve Eq. (IV.B.16) for $\ddot{\zeta}$ and substitute in Eq. (IV.B.12) for $\dot{\gamma}$ we get

$$\ddot{\zeta} = \frac{2\omega_o \dot{\gamma}}{\gamma} = \frac{2eKE\omega_o}{\gamma^2 mc} \cos(\zeta + \phi). \quad (\text{IV.B.17})$$

Define the dimensionless time as $\tau = ct/L$ so time equals zero at the beginning of the undulator and one at the end. Also define the dimensionless complex optical field $a = |a|e^{i\phi}$ where $|a| = 4\pi e NKL|E|/\gamma^2 mc^2$, so we arrive at

$$\ddot{\zeta} = |a| \cos(\zeta + \phi). \quad (\text{IV.B.18})$$

where $(\dot{\dots}) = d(\dots)/d\tau$.

We can also define the dimensionless electron phase velocity, $v = \dot{\zeta}$, where if $v = 0$, the electrons are at resonance. The electron phase velocity is proportional to the electron energy, so when v decreases, the electron is giving up energy to the optical field. The maximum energy loss from the electrons occurs when $\cos(\pi) = -1$ or when electrons are bunched at $\zeta + \phi = \pi$.

C. WAVE EQUATION

The development of a complex optical wave equation starts from Maxwell's wave equation acting on a optical vector potential $\vec{A}(\vec{r}, t)$ that is driven by a current density \vec{J}_\perp ,

$$\left[\vec{\nabla}^2 - \frac{1}{c^2} \frac{\partial^2}{\partial t^2} \right] \vec{A}(\vec{r}, t) = -\frac{4\pi}{c} \vec{J}_\perp, \quad (\text{IV.C.1})$$

where $\vec{\nabla}^2 = \partial^2/\partial x^2 + \partial^2/\partial y^2 + \partial^2/\partial z^2$. The vector potential $\vec{A}(z, t)$ for the helical FEL is

$$\vec{A}(z, t) = \frac{c}{\omega} E(z, t) [\sin(kz - \omega t + \phi(z, t)), \cos(kz - \omega t + \phi(z, t)), 0] \quad (\text{IV.C.2})$$

where the electric field \vec{E} is

$$\vec{E} = E(z, t) [\cos(kz - \omega t + \phi(z, t)), -\sin(kz - \omega t + \phi(z, t)), 0], \quad (\text{IV.C.3})$$

and

$$\bar{E} = -\frac{1}{c} \frac{\partial \bar{A}}{\partial t} . \quad (\text{IV.C.4})$$

Since the plane wave is traveling in the z direction, $\nabla^2 = \partial^2/\partial z^2$ and the operator of Eq. (IV.C.1) becomes

$$\left[\frac{\partial^2}{\partial z^2} - \frac{1}{c^2} \frac{\partial^2}{\partial t^2} \right] . \quad (\text{IV.C.5})$$

The first derivative and second derivatives of the vector potential $\bar{A}(z, t)$ with respect to z , give

$$\begin{aligned} \frac{\partial^2}{\partial z^2} \bar{A} &= \frac{1}{k} \frac{\partial E}{\partial z} \left[k + \frac{\partial \phi}{\partial z} \right] [\cos(\Psi), -\sin(\Psi), 0] \\ &+ \frac{1}{k} \frac{\partial^2 E}{\partial z^2} [\sin(\Psi), \cos(\Psi), 0] + \frac{1}{k} \frac{\partial E}{\partial z} \left[k + \frac{\partial \phi}{\partial z} \right] [\cos(\Psi), -\sin(\Psi), 0] \\ &+ \frac{E}{k} \frac{\partial^2 \phi}{\partial z^2} [\cos(\Psi), -\sin(\Psi), 0] + \frac{E}{k} \left(k + \frac{\partial \phi}{\partial z} \right)^2 [-\sin(\Psi), -\cos(\Psi), 0] . \quad (\text{IV.C.6}) \end{aligned}$$

Assume that the amplitudes and phases vary slowly with respect to time and distance traveled along the z axis so that E and ϕ change slowly: $\partial E/\partial z \ll kE$, $\partial \phi/\partial z \ll k\phi$, $\partial E/\partial t \ll \omega E$, $\partial \phi/\partial t \ll \omega \phi$, and $\omega = kc$. This allows us to use only the first-order derivatives because the second-order derivatives are small and Eq. (IV.C.6) simplifies to

$$\frac{\partial^2}{\partial z^2} \bar{A} \approx 2 \frac{\partial E}{\partial z} [\cos(\Psi), -\sin(\Psi), 0] + E \left(k + 2 \frac{\partial \phi}{\partial z} \right) [-\sin(\Psi), -\cos(\Psi), 0] \quad (\text{IV.C.7})$$

Taking the second time derivative of the vector potential $\bar{A}(z, t)$

$$\frac{\omega}{c} \frac{\partial^2}{\partial t^2} \bar{A} = \frac{\partial E}{\partial t} \left[\frac{\partial \phi}{\partial t} - \omega \right] [\cos(\Psi), -\sin(\Psi), 0] + \frac{\partial E^2}{\partial t^2} [\sin(\Psi), \cos(\Psi), 0]$$

$$\begin{aligned}
& + \frac{\partial E}{\partial t} \left[\frac{\partial \phi}{\partial t} - \omega \right] [\cos(\psi), -\sin(\psi), 0] + E \frac{\partial \phi^2}{\partial t^2} [\cos(\psi), -\sin(\psi), 0] \\
& + E \left[\frac{\partial \phi}{\partial t} - \omega \right]^2 [-\sin(\psi), -\cos(\psi), 0]. \quad (\text{IV.C.8})
\end{aligned}$$

The amplitudes and phases are both slowly-varying and we ignore second-order derivatives. If we also multiply by $1/c^2$, Eq. (IV.C.8) becomes

$$\frac{1}{c^2} \frac{\partial^2}{\partial t^2} \vec{A} \approx -2 \frac{1}{c} \frac{\partial E}{\partial t} [\cos(\psi), -\sin(\psi), 0] + \frac{1}{c} (\omega E - 2E \frac{\partial \phi}{\partial t}) [-\sin(\psi), -\cos(\psi), 0] \quad (\text{IV.C.9})$$

Recombine the two halves so we have

$$\begin{aligned}
& \left[\nabla^2 - \frac{1}{c^2} \frac{\partial^2}{\partial t^2} \right] \vec{A} \approx 2 \left[\frac{\partial E}{\partial z} + \frac{1}{c} \frac{\partial E}{\partial t} \right] [\cos(\psi), \sin(\psi), 0] \\
& + 2E \left[\frac{\partial \phi}{\partial z} + \frac{1}{c} \frac{\partial \phi}{\partial t} \right] [-\sin(\psi), -\cos(\psi), 0]. \quad (\text{IV.C.10})
\end{aligned}$$

Define dimensionless time $\tau = ct/L$ so that τ equals zero at the beginning of the undulator and one at the end. Follow a new position $z \rightarrow z + ct$ and use the chain rule to simplify the operator for the wave equation:

$$-\frac{4\pi}{c} \vec{J}_\perp \approx 2 \left[\frac{1}{L} \frac{\partial E}{\partial \tau} \right] [\cos(\psi), \sin(\psi), 0] + 2E \left[\frac{1}{L} \frac{\partial \phi}{\partial \tau} \right] [-\sin(\psi), -\cos(\psi), 0] \quad (\text{IV.C.11})$$

As for the right side of the equation, we know the current density for a single electron is $\vec{J}_\perp = -ec\vec{\beta}_\perp$. From Eq. (IV.B.11), the electron trajectory, we have

$$\vec{J}_\perp = \frac{eCK}{\gamma} [\cos(k_o z), \sin(k_o z), 0] \quad (\text{IV.C.12})$$

where K is the undulator parameter, k_o is the undulator wave number, and γ is the Lorentz factor. Eq. (IV.C.12) is substituted into Eq. (IV.C.11) to get

$$\begin{aligned}
& -\frac{4\pi eK}{\gamma} [\cos(k_o z), \sin(k_o z), 0] \approx \\
& 2 \left[\frac{1}{L} \frac{\partial E}{\partial \tau} \right] [\cos(\Psi), \sin(\Psi), 0] + 2E \left[\frac{1}{L} \frac{\partial \phi}{\partial \tau} \right] [-\sin(\Psi), -\cos(\Psi), 0] \quad (\text{IV.C.13})
\end{aligned}$$

Eq. (IV.C.13) can be separated using two unit vectors representing change in E and change in ϕ

$$\frac{\partial E}{\partial \tau} = -\frac{2\pi eLK}{\gamma} [\cos(k_o z), \sin(k_o z), 0] \cdot [\cos(\Psi), \sin(\Psi), 0], \quad (\text{IV.C.14})$$

which becomes

$$\frac{\partial E}{\partial \tau} = -\frac{2\pi eLK}{\gamma} \cos(\zeta + \phi), \quad (\text{IV.C.15})$$

where ζ is the electron phase $(k+k_o)z - \omega t$. Performing the same steps for $\partial\phi/\partial\tau$ gives

$$\frac{\partial \phi}{\partial \tau} = \frac{2\pi eLK}{\gamma} \sin(\zeta + \phi). \quad (\text{IV.C.16})$$

Eq. (IV.C.15) and Eq. (IV.C.16) are the wave equation driven by single electrons. A more useful equation uses the sum over many electrons in the FEL beam. This can be done by taking the average $\langle \dots \rangle$ and multiplying by the electron particle density, ρ , resulting in

$$\frac{\partial E}{\partial \tau} = -\frac{2\pi e\rho LK}{\gamma} \langle \cos(\zeta + \phi) \rangle, \quad (\text{IV.C.17})$$

$$\frac{\partial \phi}{\partial \tau} = \frac{2\pi e \rho L K}{\gamma} \langle \sin(\zeta + \phi) \rangle. \quad (\text{IV.C.18})$$

Taking the derivative of the complex electric field $E = |E|e^{i\phi}$ with respect to dimensionless time, τ , and insert Eq. (IV.C.17) and Eq. (IV.C.18) as appropriate, to get

$$\frac{\partial E}{\partial \tau} = -\frac{2\pi e \rho L K}{\gamma} [\langle \cos(\zeta + \phi) \rangle - i \langle \sin(\zeta + \phi) \rangle] e^{i\phi}, \quad (\text{IV.C.19})$$

which can be further simplified

$$\frac{\partial E}{\partial \tau} = -\frac{2\pi e \rho L K}{\gamma} \langle e^{-i\zeta} \rangle. \quad (\text{IV.C.20})$$

And from the pendulum equation, we know that our dimensionless optical wave field is $a = |a|e^{i\phi}$, where $|a| = 4\pi e N K L |E| / \gamma^2 mc^2$, so that the wave equation is now

$$\frac{\partial a}{\partial \tau} = \dot{a} = -j \langle e^{-i\zeta} \rangle, \quad (\text{IV.C.21})$$

where the dimensionless current is $j = 8\pi^2 e^2 \rho N K^2 L^2 / \gamma^3 mc^2$. The growth of the optical field depends on the dimensionless current, j , and the electron phase average. If there is no current or no electron bunching, then there is no growth of the optical field.

D. LOW GAIN FEL

Combining the pendulum equation, derived from the relativistic Lorentz force equations, and the optical field wave equation, derived from Maxwell's wave equation, yields a result valid for either low gain or high gain, and weak or strong optical fields. Low gain occurs when the dimensionless current is small, $j < \pi$, and there is little change in the value of the optical field, $a \approx 0$. Weak fields are defined by a small dimensionless optical field, or $|a| < \pi$ where there is not much change in the electron phase velocity, v .

When designing a weapon system the FEL should have a high average power. The current world record for the highest average power FEL is a low gain design located at the Thomas Jefferson National Accelerator Facility, TJNAF. An FEL having low gain typically operates as an FEL oscillator that takes many passes through the undulator in order to build an optical field within the resonator. Single-pass gain is defined as the fractional change in optical power as it makes a single pass down the undulator

From the conservation of energy, the change in the electron pulse energy is converted to a change in the optical pulse energy. The energy of a relativistic electron is equal to γmc^2 , and the change in an electron's energy is $\Delta\gamma mc^2$. Near resonance, small changes in the electron phase velocity, v , are given by $\Delta v = 4\pi N \Delta\gamma/\gamma$ [26]. The energy change of a single electron is

$$\Delta\gamma mc^2 = \frac{\gamma mc^2 \Delta v}{4\pi N}. \quad (\text{IV.D.1})$$

Since we are dealing with a pulse rather than a single electron, we can assume an average phase velocity for all the electrons within the pulse, $\langle v \rangle$. Therefore the average change in electron beam energy is

$$\overline{\Delta\gamma mc^2} = \frac{\gamma mc^2 (\langle v \rangle - v_o)}{4\pi N}. \quad (\text{IV.D.2})$$

With low gain in weak fields, the optical phase, ζ , can be written as a power series in a_o using perturbation theory [26],

$$\zeta(0) = \zeta_o + v_o \tau - \frac{a_o}{v_o^2} [\cos(\zeta_o + v_o \tau) - \cos(\zeta_o) + v_o \tau \sin(\zeta_o)] + \dots \quad (\text{IV.D.3})$$

where ζ_o is the initial electron phase, v_o is the initial electron phase velocity, and a_o is the initial optical field amplitude. Since the electron phase velocity, v , equals the derivative of ζ with respect to τ , it also can be written as a power series in a_o using perturbation theory,

$$\begin{aligned} v(\tau) = v_o + \frac{a_o}{v_o} [\sin(\zeta_o + v_o \tau) - \sin(\zeta_o)] \\ + \frac{a_o^2}{v_o^3} \left[-\frac{1}{4} (\cos(2\zeta_o + 2v_o \tau) - \cos(2\zeta_o)) + \cos(v_o \tau) \right. \\ \left. - 1 - v_o \tau \sin(\zeta_o) \cos(\zeta_o + v_o \tau) \right] + \dots, \end{aligned} \quad (\text{IV.D.4})$$

By averaging over a uniform distribution of the initial electron phases in the beam, average phase change is

$$\langle v \rangle = v_o t \frac{a_o^2}{v_o^3} \left[\cos(v_o \tau) - 1 + \frac{1}{2} v_o \tau \sin(v_o \tau) \right]. \quad (\text{IV.D.5})$$

The number of electrons in the beam is equal to the electron density, ρ , multiplied by the elemental volume unit, dV . Since the electron beam only amplifies the light within the area where the two beams overlap, a filling factor, F , must be included. The filling factor is the area of the electron beam divided by the larger area of the light beam,

$$F = \frac{r_b^2}{w_o^2}, \quad (\text{IV.D.6})$$

where r_b is the electron beam radius and w_o is the radius of the optical beam waist. The average change in the electron beam energy is then

$$\overline{\Delta \gamma m c^2} = \frac{(\rho F dV)(\gamma m c^2)(\langle v \rangle - v_o)}{4\pi N}. \quad (\text{IV.D.7})$$

Since gain is defined as the change in optical wave energy divided by the initial optical wave energy, the increase in optical wave energy is equal to the decrease in the electron beam energy. The gain, G , is calculated by dividing the change in electron beam energy by the initial optical wave energy within dV , $2E^2 dV/8\pi$. Substituting Eq. (IV.D.5) and Eq. (IV.D.6) into Eq. (IV.D.7), we can solve for gain

$$G = j \frac{[2 - 2 \cos(\nu_o \tau) - \nu_o \tau \sin(\nu_o \tau)]}{\nu_o^2}, \quad (\text{IV.D.8})$$

where $j = 8N(e\pi KL)^2 \rho F/\gamma^3 mc^2$ is the dimensionless current density. Using Eq. (IV.D.8) and a dimensionless current density of $j = 1$, gives a plot of gain versus initial electron phase velocity, ν_o , can be constructed. The plot, see Figure (21), shows that for an initial electron phase velocity of $\nu_o = 0$ the gain, G , will be zero, due to an equal number of electrons gaining and losing energy. The gain, G , increases, reaching a maximum value at $\nu_o = 2.6$, because more electrons lose energy than gain. Then gain decreases to $G = 0$ at $\nu_o \gg 1$ as the electron phase and optical phase have less and less interaction due to the high initial electron phase velocity. The antisymmetry of Figure (21) shows that if $\nu_o < 0$ then the gain, G , will be negative because the electrons will have a net gain of energy from the optical pulse. Eq. (IV.D.8) shows the gain, G , is also proportional to the dimensionless current density, j . For increasing values of j the amplitude of the optical pulse increases, the optical pulse width narrows and short pulse effects are increased.

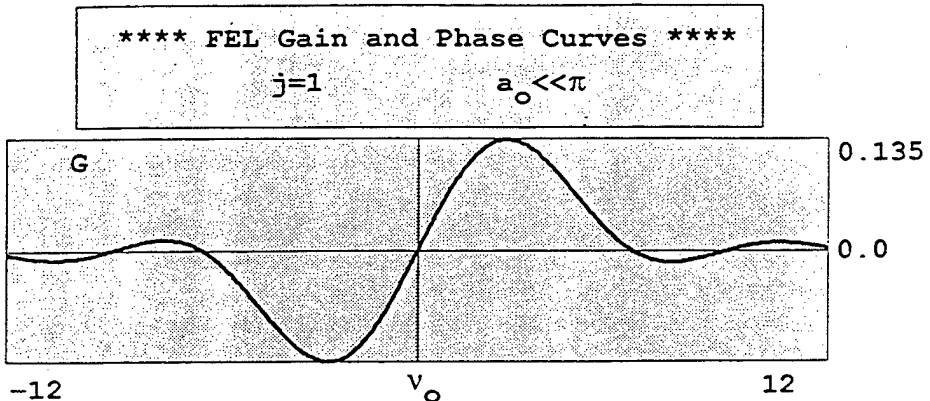


Figure 21. Low Gain Spectrum for Low Current and Weak Fields [26]

E. SHORT PULSE EFFECTS

FEL oscillators in general use short electron pulses rather than a continuous beam. Recall that near resonance one wavelength of light passes over an electron as the electron travels one undulator wavelength. In the time the electron pulse travels the length of the undulator, it has slipped behind the light pulse by $N\lambda$, this distance is defined as the "slippage distance". If the electron pulse is much longer than the slippage distance, then each part of the electron pulse experiences different gain due the different local electron density, ρ , and would have to be treated accordingly. FEL amplifiers typically have electron pulses that are much longer than the slippage distance. In the FEL oscillator, the electron pulse length is often on order of the slippage distance, so that the electron and optical pulses actually pass over each other.

An effect that stems from the short pulses in an FEL oscillator is known as "lethargy"[26]. The light pulses are bounced between resonator mirrors separated by a distance, S , which is greater than the length of the undulator. Taking a time, $t=2S/c$ to complete a full cycle. In order to maintain the FEL interaction the bounce time of the

laser pulses must be synchronized with the sequence of electron pulses from the accelerator so that the electron and optical pulses enter the undulator together. When the pulses are timed to arrive exactly together at the beginning of the undulator, this condition is called exact synchronism, which is shown in figure (21).

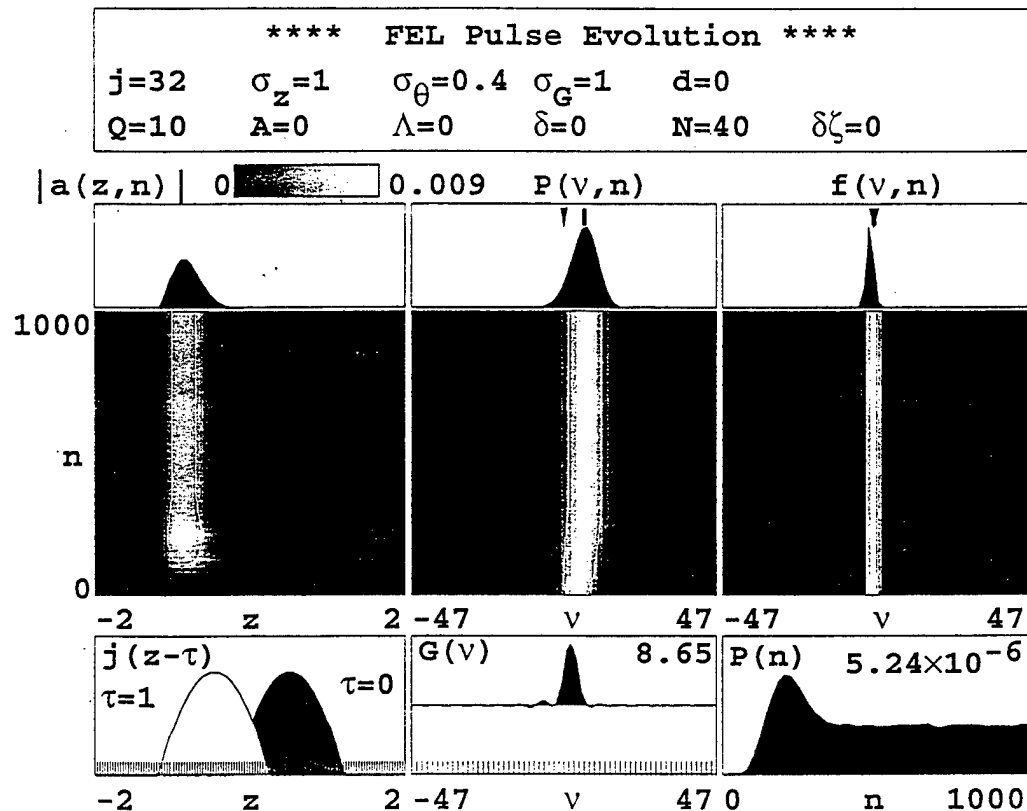


Figure 21. FEL oscillator at exact synchronism

Surprisingly, the FEL has no steady state power at exact synchronism, which can be explained in the following manner. The light pulse and the electron pulse enter the undulator together and begin to interact, but initially there is no gain, because there is no electron bunching. As the light pulse interacts with the electron pulse, the electrons in the pulse begin to bunch and gain is developed. As the pulses travel down the undulator

together gain increases. Since the light pulse moves ahead of the electron pulse the majority of the amplification is in the rear of the light pulse. The centroid of the light pulse moves back and in effect travels at a speed slightly less than c . If the two pulses start together at the beginning of the undulator, the light pulse will fall behind over many passes and the coupling between the two pulses will be lost. Eventually the resonator losses will cause the optical pulse to decay, and the FEL will fail to operate. In order for the FEL to operate, we need to advance the entry of the light pulse compared to the electron pulse. This advance is accomplished by shortening the resonator length slightly.

F. DESYNCHRONIZATION EFFECTS

Desynchronization can seriously affect the performance of the FEL.

Desynchronization is adjusted by moving one of the mirrors of the resonator cavity inward by a small amount ($\Delta S \approx 2-10 \mu\text{m}$). The value of desynchronization is given by

$$d = -\frac{2\Delta S}{N\lambda}, \quad (\text{IV.F.1})$$

where ΔS is the decrease in the distance between the mirrors. Desynchronization is normalized by the slippage distance, $N\lambda$, and gives the displacement between the electron and optical pulses at $\tau = 0$ on each pass [26].

In figure (21) desynchronization was $d = 0$ and there was no steady state power. So several computer simulations were run in order to investigate the effect desynchronization had on gain and power. In figure (22), the FEL parameters used a desynchronization of $d = 0.003$, and power reaches steady state at a substantial level as the optical pulse survives.

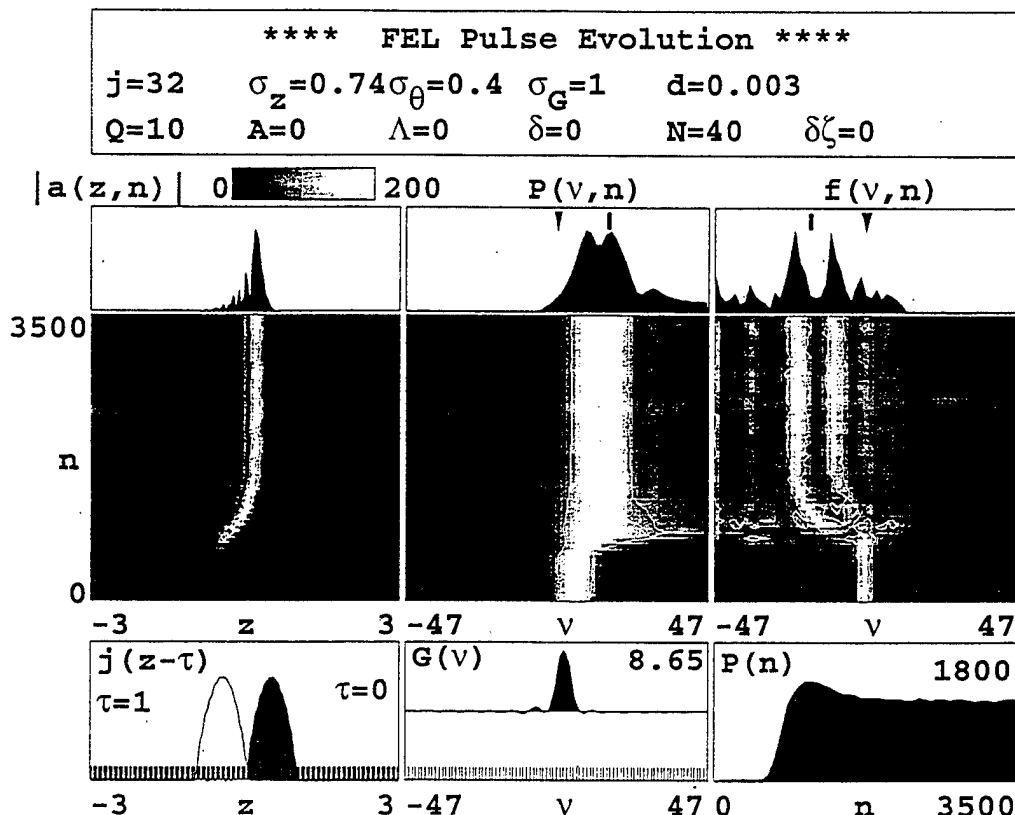


Figure 23. FEL oscillator at small desynchronization

Figure (23) shows the peak power and peak field strength, $|a| \approx 200$, are reached between $n = 800$ and $n = 1000$ passes, with steady-state power, $P(n)$, being reached after approximately $n = 1800$ passes. Figure (23) also shows the evolution to a narrow optical spectrum, $P(v,n)$, and a broad electron spectrum, $f(v,n)$. Although there appears to be a high steady-state power level, the FEL oscillator is very sensitive to small changes in d . A more detailed analysis of the effects of desynchronization for the TJNAF are included in section VI.

G. LIMIT CYCLE BEHAVIOR

Limit cycle behavior is a possible result of operating the FEL in strong fields with short pulse effects. The combination of the fields present in the undulator can result in what is known as trapped-particle instability. Trapped-particle instability is generated when the height of the separatrix is large and most electrons travel in closed paths. The electrons in the closed paths are trapped in deep potential wells and tend to oscillate at the synchrotron frequency, $\nu_s = \sqrt{|a|}$ [26]. These oscillations mix with the optical carrier frequency causing modulation of the optical wave envelope and sidebands at the synchrotron frequency. The modulation of the optical pulse shape in combination with the desynchronization effect and resonator losses creates an optical pulse that varies periodically over many passes. Figure (24) illustrates limit cycle behavior for the TJNAF FEL.

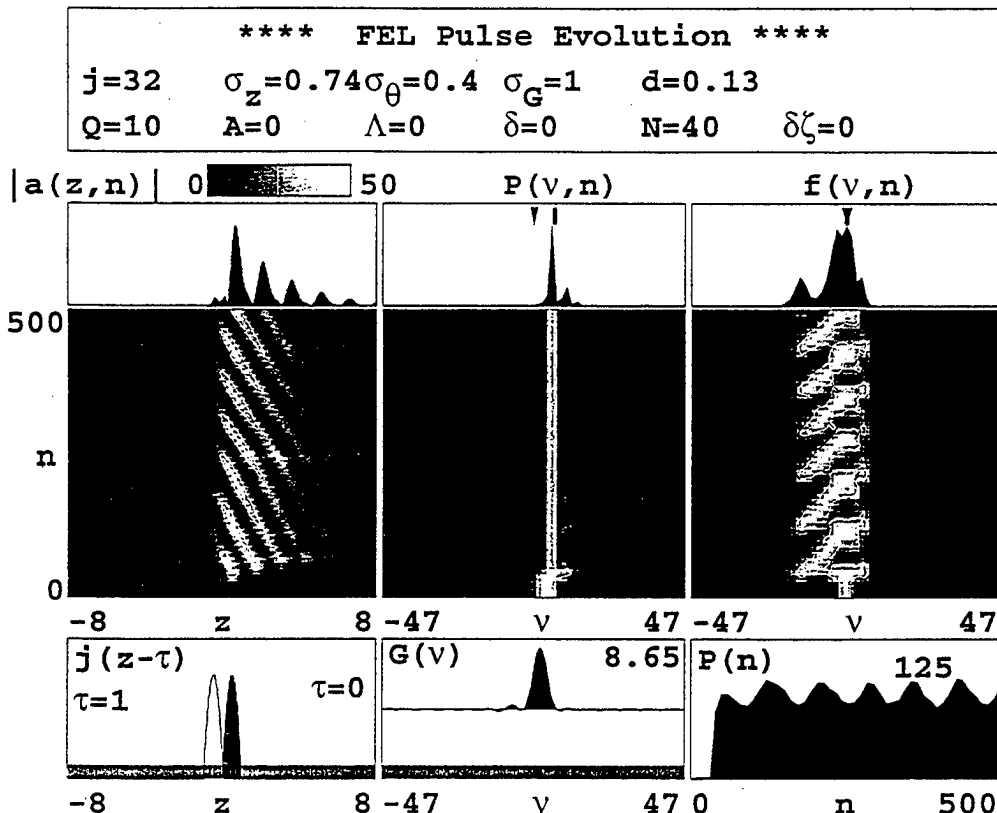


Figure 24. Example of Limit Cycle Behavior

The modulation of the optical field first grows due to slippage and desynchronization. As seen in the optical pulse evolution $|a(z,n)|$, subpulses form at the rear of the pulse due to the modulation of the optical pulse at the synchrotron frequency. Although the centroid of the optical pulse is held constant with respect to the electron pulse, the features continue to move forward in z at each successive pass. As the subpulses move forward with respect to the centroid, they first enter a region of higher gain and grow, then desynchronization moves the pulse forward where the resonator losses cause decay. The optical field amplitude oscillates as the subpulses formed in the rear of the pulse move

forward, eventually dying out in the region where there is no gain. Figure (24) shows the output power, $P(n)$, oscillating due to modulation of the optical field.

Limit cycle behavior corresponds to the creation of sidebands in the optical spectrum and widens the output light spectrum of the FEL, which can be seen in Figure (24). As discussed in section III.C.2, we need a narrow light spectrum to exploit an atmospheric propagation window. Therefore, limit cycle behavior may be an undesired effect. Fortunately, FEL designers understand limit cycle behavior well enough to control its by simply altering desynchronism.

V. LASER MATTER INTERACTION

A. CONTINUOUS WAVE LASERS

We have discussed the generation of laser energy and its propagation through the atmosphere. We now consider what happens when the laser energy strikes the target. Of primary interest is the laser matter interaction at the surface of the missile. When the laser energy strikes the material, some of the energy is absorbed and some is reflected. The absorbed energy causes a rise in the surface temperature. If sufficient energy is deposited, the material melts and the laser beam bores through the material. The required energy per unit area [27, 28] is

$$E_o = \rho d [C(T_M - T_0(1 + 0.2M^2)) + \Delta H_M],$$

where ρ is the density of target material, d is the target thickness, C is the specific heat of the material, T_M is the melting temperature, T_0 is the ambient air temperature, M is the mach number of the missile, $T_0(1 + 0.2M^2)$ is the temperature of the missile nose traveling at mach speed M , and ΔH_M is the heat of melting of the material. For aluminum traveling at mach speed $M = 1$, we find that an energy density, $E_o \approx 3000 \text{ J/cm}^2$ is needed for melting aluminum. If the power density at the target from a laser weapon is taken to be $1 \text{ MW over } 100 \text{ cm}^2$, or 10 kW/cm^2 , it would take approximately one-third of a second to provide sufficient energy to melt through one centimeter of aluminum, if all the energy were absorbed. With a one second dwell time, a substantial fraction of the incident power can be reflected as long as 3000 J/cm^2 is absorbed. For a Mach 2 missile, the

energy density needed to melt the aluminum is only $E_o \approx 2000 \text{ J/cm}^2$ since the missile is already hot, so faster missiles require shorter dwell times or less power.

B. SHORT LASER PULSES

Short pulsed lasers, microseconds or shorter, are capable of producing impulse damage in addition to the thermal damage. When the laser power is delivered in pulses, the peak power increases and may cause new effects beyond thermal heating. Due to the higher peak laser energy, there can be rapid vaporization at the target surface, so that a strong pressure wave is formed by the recoil from the vapor blowoff. The peak of the pressure wave, or impulse, induces a shock front, while the rear of the wave induces a rarefaction wave. The shock front reflects when it reaches a free surface at the rear of the material. The superposition of the reflected and incident waves results in stress at the free surface, which can exceed the material strength causing spalling. [29]

Figure (25) is an example of the result of spalling in a 25 μm thick MetGlass sample due to impulse delivered by a single 2.2ns, 26 J laser pulse at $\lambda = 1.06 \mu\text{m}$ wavelength focused to a 500 μm spot [30].

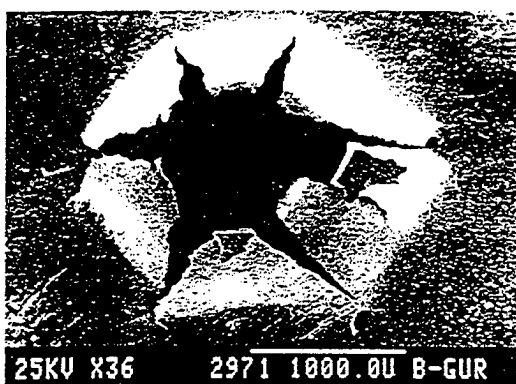


Figure 25. Spalling in Metglass

Creation of a vapor at the material's surface is necessary for impulse generation leading to spalling damage. Assuming the thickness of the material exceeds the thermal diffusion length, $D = 2(\kappa t_p)^{1/2}$, where κ is the thermal diffusivity equal to cm^2/s and t_p is the laser pulse length, a rough estimate for the onset of vaporization requires an energy density $E_o \geq D\rho L_v$, where L_v is the heat of vaporization [31]. For an one picosecond laser pulse, the thermal diffusion length in aluminum is $D \approx 2 \mu\text{m}$. Using 1 MW over 100cm^2 on target and a pulse length of a few picoseconds for an FEL laser weapon, we find that no vapor is formed so there would be no impulse or spalling damage.

C. ULTRA-SHORT LASER PULSES

In recent years, new laser capabilities have allowed damage research with ultra-short laser pulses, from picosecond to femtoseconds. Ultra-short laser pulse lengths deliver energy to a metal at such a fast rate that the metal lattice cannot respond, but the electrons can [34]. The electrons rapidly increase in temperature so that the difference between electron and lattice temperatures can be as much as a few thousand degrees. Eventually, electron-phonon interactions distribute the excess energy between the electrons and the lattice in a time equal to a few phonon oscillation periods, a few to tens of picoseconds [35]. Higher fluences produce larger temperature differences between the electrons and the lattice, so that more electron-phonon collisions are required for thermalization [36].

A theory developed to describe the effect of pulse-duration on optical damage to metals argues that with ultra-short pulses, the electrons penetrate the material to a certain heat deposition depth before coupling to the lattice [37]. For pulses shorter than the

lattice relaxation time, the heat-deposition depth is relatively large and the resulting damage threshold fluence, E_{th} , is independent of pulse duration. For pulse lengths longer than a critical time, τ_c , which is larger than the relaxation time by a factor of $C/C_e T_M$ where C is the material heat capacity, C_e is the electron heat capacity, T_M is the melting temperature, the diffusion of energy to the lattice becomes important. In this case, E_{th} will scale as the square root of the pulse length, $(\tau_p)^{1/2}$ [38-40]. Figure (26) shows the dependence of the damage threshold fluence, E_{th} , on pulse length for Cu and Mo [40]. The experimental results show a lower damage threshold fluence, E_{th} , as the pulse length is decreased down to one picosecond. For pulses shorter than one picosecond, E_{th} becomes independent of pulse length. Figure (26) implies that there may be as much as a factor of ten advantage when using shorter picosecond pulses over larger 100 nanosecond pulses.

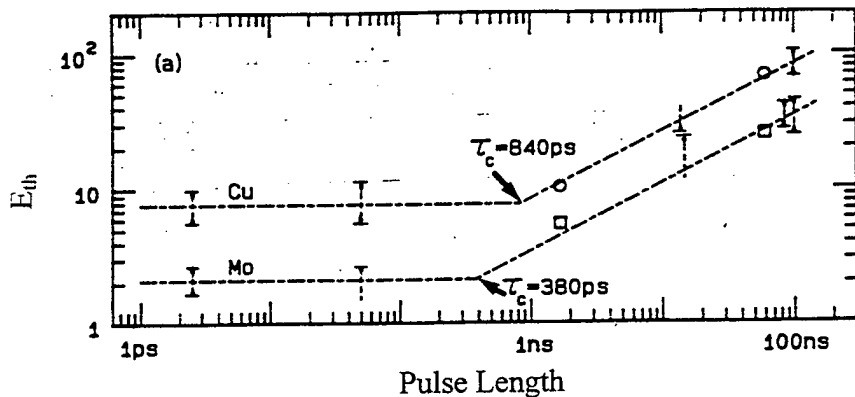


Figure 26. Damage threshold energy vs. pulse length [40]

Research has also examined the threshold for ultra-short pulses damaging dielectrics [41, 42]. Figure (27) [42], shows the same basic trend as with Figure (26) for

metals. For long nanosecond pulses, the damage threshold decreases with decreasing pulse length as $(\tau_p)^{1/2}$ and does not depend on pulse length for very short, picosecond pulses. The critical pulse length, τ_c , for the transition was hundreds of picoseconds for metals, but is only a few picoseconds for dielectrics. As with metals, it appears that there may be as much as a factor of ten advantage when using shorter picosecond pulses compared to longer nanosecond pulses.

From these studies, it may be inferred that there is the possibility of decreasing the fluence required to cause damage to a material with ultra-short picosecond pulses compared to cw or short nanosecond pulses. If this is true, then it may be possible that the energy required to damage an in-bound missile could be significantly reduced. The advantage could decrease the size of the FEL required on-board ship, decrease the possibility of thermal blooming because of lower propagating power, and decrease the dwell time on target.

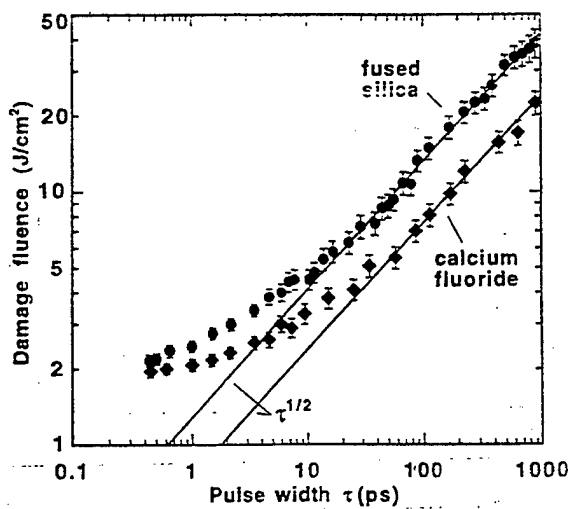


Figure 27. Damage Fluence vs. Pulse Width for Dielectrics

VI. THOMAS JEFFERSON NATIONAL LABORATORY

FELs producing kilowatt average power do not yet exist, and it will be many years before the FEL will be usable as a laser weapon for the Navy's needs. However, the TJNAF FEL is an important step in that direction. Two years after breaking ground and beginning construction, the TJNAF FEL achieved first-light on June 17, 1998 producing 155 W of cw power. This eclipsed the previous record of 11 W held by Vanderbilt University. In late November 1988, the TJNAF FEL more than doubled its average power to 340W. In the near future, the TJNAF's goal is to achieve 1 kW, and then move on to a goal of 20 kW.

Figure (28) shows the basic design of the current laser. Figure (29) shows the modification planned for the 20kW infrared wavelength FEL and a 1kW ultraviolet wavelength FEL. Currently, the electrons are supplied by a 350 keV photocathode gun that are accelerated first by a 10 MeV superconducting cyromodule, then by a 47 MeV superconducting accelerator, to achieve a 57 MeV electron beam energy. The electrons then enter the undulator, or "wiggler", to amplify the copropagating laser light as described in section IV. The wiggler covers the wavelength range from $\lambda = 3.0$ to $6.6 \mu\text{m}$ using $N = 40$ periods of $\lambda_o = 2.7 \text{ cm}$. The initial results achieving 340 W did not recirculate the electron beam. When energy recirculation at full current is achieved in the future, the estimated power output at $\lambda = 3 \mu\text{m}$ wavelength is 980 W or about 1kW. TJNAF has achieved 124 W output power using partial current in their recirculation ring. The recirculation ring will eventually play an important role as it is designed take the

electrons from the output of the wiggler, and send them back through the 47 MeV cyromodule, which would then act as a decelerator to recover the electron beam energy. This conserves energy by using "spent" electrons to help feed RF power to the cyromodule, and also reduces the beam dump shielding since significant energy is extracted from the electrons. These two features make the use of recirculation attractive for future shipboard designs.

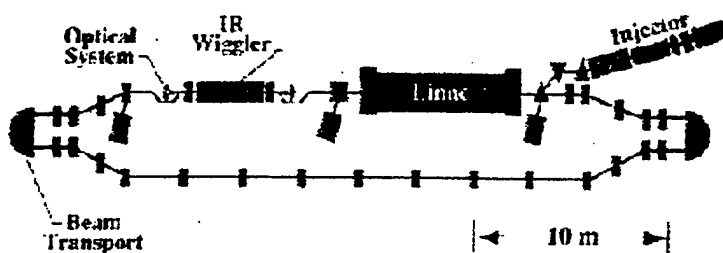


Figure 28. Diagram of current TJNAF FEL

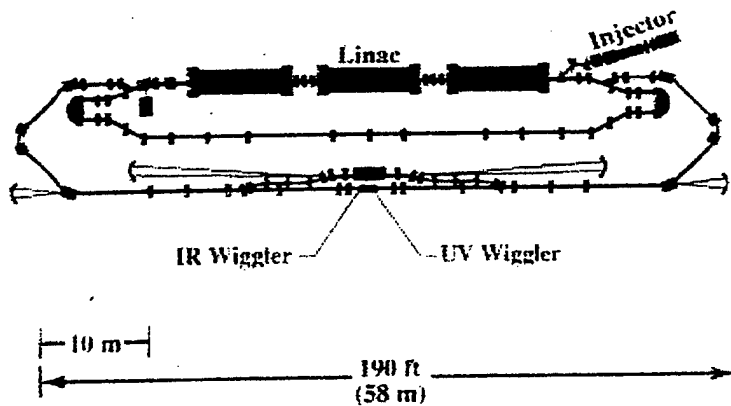


Figure 29. Diagram of Envisioned TJNAF FEL

The performance of the current TJNAF FEL is now studied using simulations. Desynchronization, discussed in section IV.E, has an important effect on output power and optical pulse shape. It is one of the parameters used to control limit-cycle behavior, as discussed in section IV.F.

In these simulations, TJNAF FEL electron pulse bunch length is taken to be 100-200 μm , the length of the resonator is 801 cm, the resonator losses are 10%, the number of undulator periods is $N = 40$, the undulator parameter is $K = 0.96$, the undulator wavelength is $\lambda_o = 2.7$ cm. The rayleigh length is 40 cm, the electron charge per bunch is $I_e/c = 60$ pC, the pulse repetition rate is 18.725 MHz, and the electron energy is $\gamma mc^2 \cong 38\text{MeV}$. The Lorentz factor is the ratio of electron energy to the electron rest mass energy and is $\gamma = 75$. The electron pulse length is estimated in the range of 0.33-0.66 ps. The peak current estimated from the charge per bunch and pulse length is 90-180 amps depending on the pulse length taken. The value of desynchronism, $d = \Delta S/N\lambda$, was varied to see the various effects on optical power and gain.

Figure (30), shows that large and small values of desynchronism result in small gain. Since desynchronism controls the coupling of the electron and optical pulses over many passes, if desynchronism is too large or too small there will not be efficient coupling. A maximum gain of almost $G \cong 300\%$ was found to occur at desynchronism of $d \cong 0.3$.

Gain vs. Desynchronism

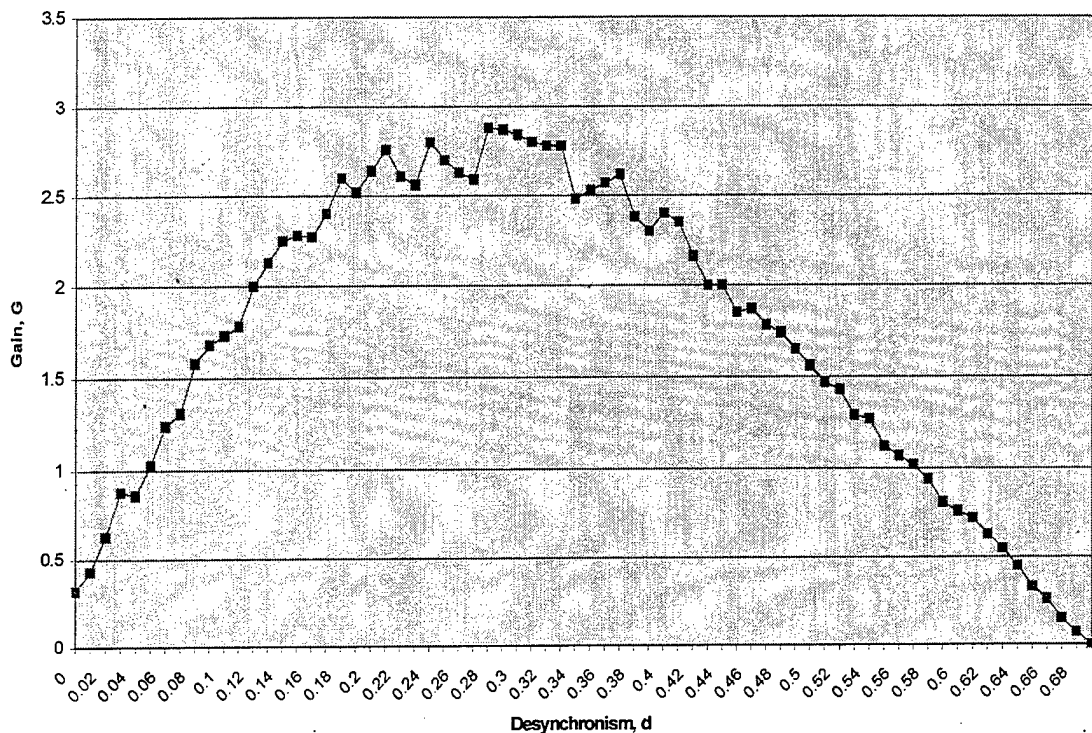


Figure 30. Gain vs. Desynchronism

The values of the electron pulse length and therefore the pulse peak current are not accurately known in the TJNAF experiment so that a range of values is used in the simulations. Pulse lengths of 0.33 ps, 0.4 ps, 0.45 ps, 0.5 ps, 0.6 ps were used and the corresponding peak current was varied to keep the total pulse charge the same. Graphs of power level vs. desynchronism for each pulse length were constructed. As the pulse length decreases, coupling is reduced because of lethargy. But, higher peak current for a shorter pulse compensates. Figure (31), shows the steady-state optical power as desynchronism is varied over small values. Superimposed are the results of each of the pulse lengths sampled.

Power vs. Desynchronism

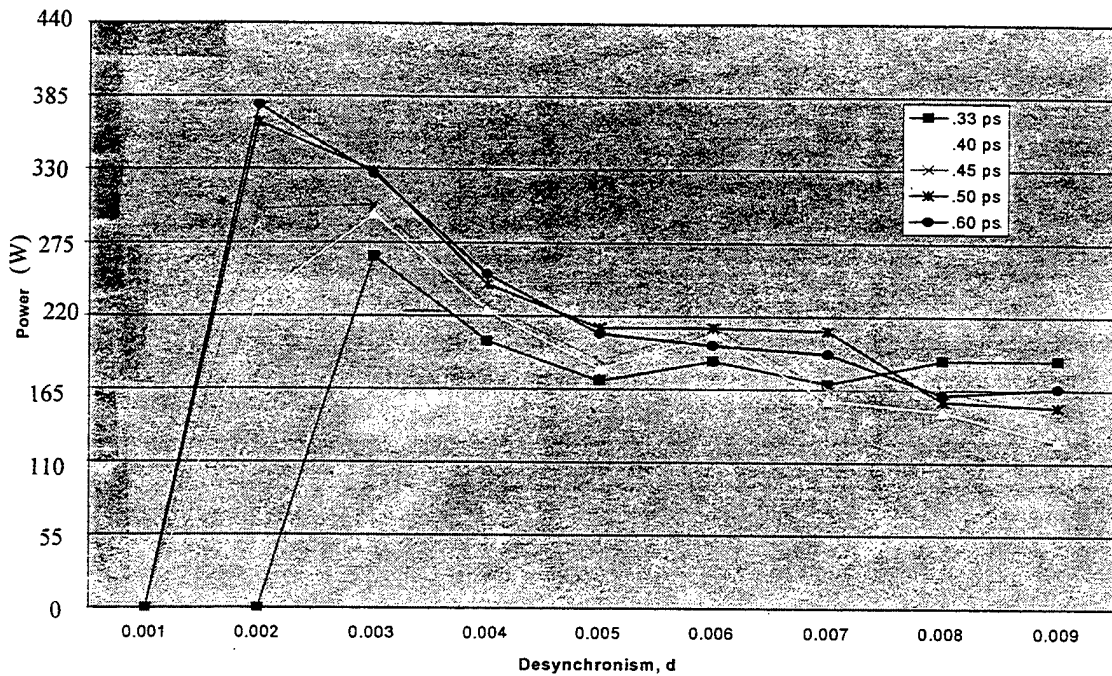


Figure 31. A composite of Power vs. Desynchronism

At low values like $d \approx 0.001$ the power initially increases rapidly, with increasing desynchronism. The simulations indicate an average power of 324 W, which is in close agreement with the observed average power of 340 W, when TJNAF set the FEL record. More stable operation is formed for values of $d > 0.1$, shown in figure (32). As d increases past $d \approx 0.04$, power steadily decreases. Simulations were also run for $d > 0.2$, and the power levels slowly decreased until finally reaching a zero power level at $d \approx 0.7$.

Power vs. Desynchronization

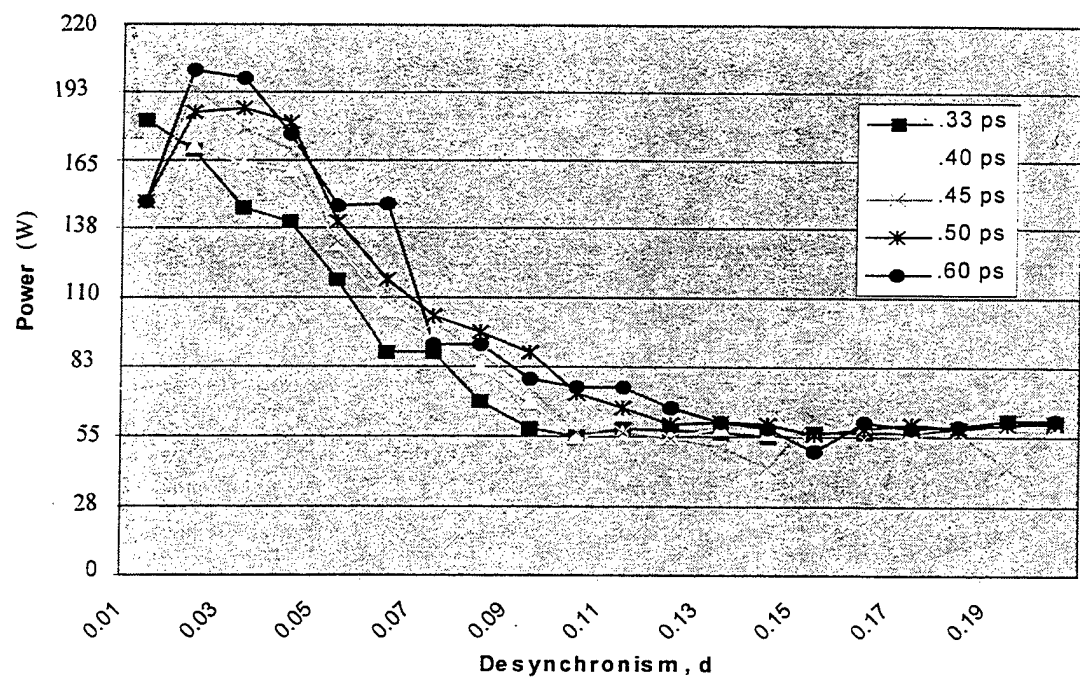


Figure 32. A composite of Power vs. Desynchronization

VII. CONCLUSIONS

The thesis investigates ship self-defense against anti-ship missiles. The kinetic energy weapon systems were found not suitable for ship defense in the future. Computer simulation determined that CIWS is inadequate for current threats. When defensive missiles engage inbound missiles prior to terminal maneuvers, they can be successful. However, the Navy's current role requires ships to operate within the littoral region for gunfire support. This places the ship inside the effective range of the standard missile. So that the ship's flexibility would be curtailed in order to ensure ship safety.

Two promising kinetic energy weapons were evaluated: long wavelength high power microwaves (HPM) and short wavelength lasers. Diffraction at long wavelengths spreads the HPM energy over a large area reducing intensity, and shielding the missile appears to be a simple, non-costly procedure.

Short wavelength laser weapons were also studied. MIRACL and ALL have already demonstrated the effectiveness of laser weapons, but thermal blooming in stagnant air and adverse weather conditions limit atmospheric propagation of the laser beam at the wavelengths used. The FEL's ability to select a particular wavelength can significantly reduce thermal blooming in maritime conditions. The tunable FEL mechanism allows changes in wavelength without significant redesign.

It is shown that MW FEL could produce significant damage, and the required power decreases as missile speed increases over Mach 1. As a result of analysis in this thesis, it is proposed that the FEL's ultra-short pulse may reduce the amount of energy required to damage a missile. If less energy is necessary for damage, the chance of

thermal blooming may be reduced. A combination of wavelength selection and ultra-short pulse effect may significantly reduce the thermal blooming problem, reduce the size of the FEL weapon, decrease the dwell time, or increase the probability of kill.

The FEL appears to be the best laser weapon choice at this time, but since FEL technology is relatively new, an FEL capable of delivering the required power is still years away. To aid in the furthering FEL science and to help develop an FEL the performance of TJNAF FEL is investigated. The simulations performed for and described in this thesis describe the expected performance of the TJNAF FEL for many values of electron pulse length, peak current and cavity desynchronization. These simulations are used to explain recent experimental observations of the TJNAF FEL.

In conclusion, it is recommended that ultra-short pulse effects on missile radome materials be further investigated experimentally and theoretically. This investigation can be done with existing lasers such as the TJNAF FEL using a small target cross-section at a relatively low cost. The necessary power density of 10 kW/cm^2 can be achieved over a 1 mm^2 spot with a 100 W FEL.

LIST OF REFERENCES

- [1] J.Benford and J. Swegle,*High-Power Microwaves*, Artech House, Norwood, MA, 1991, p.16.
- [2] W.B.Colson, Physics 4911 Course Notes, Naval Postgraduate School, 1997
- [3] B. Graham, "Antimissile Test Yields 5th Failure In A Row", Washington Post, May 13, 1998.
- [4] W.F.Wilkenson, "A Theory for Optical Wavelength Control in Short Pulse Free Electron Laser Oscillators",Master's Thesis, Naval Postgraduate School, June 1993.
- [5] R.W. Duffner, *Airborne Laser: Bullets of Light*, Plenum Trade, New York and London, 1993, pp.279-310.
- [6] J.R. Cook and J.R. Albertine, "High Energy Laser Weapon System", *Surface Warfare*, September/October 1997, Vol.22, N0.5.
- [7] C.D. Taylor and D.V. Giri,*High-Power Microwave Systems and Effects*, Taylor and Francis, Washington DC, 1994, pp.198.
- [8] J.Benford and J. Swegle,*High-Power Microwaves*, Artech House, Norwood, MA, 1991, pp.5-12.
- [9] J.Benford and J. Swegle,*High-Power Microwaves*, Artech House, Norwood, MA, 1991, p.18.
- [10] C.D. Taylor and D.V. Giri,*High-Power Microwave Systems and Effects*, Taylor and Francis, Washington DC, 1994, p.19.
- [11] J.Benford and J. Swegle,*High-Power Microwaves*, Artech House, Norwood, MA, 1991, pp.21.
- [12] J.Benford and J. Swegle,*High-Power Microwaves*, Artech House, Norwood, MA, 1991, pp.115.
- [13] J.Benford and J. Swegle,*High-Power Microwaves*, Artech House, Norwood, MA, 1991, pp.20-23.
- [14] J.Benford and J. Swegle,*High-Power Microwaves*, Artech House, Norwood, MA, 1991, pp.20.
- [15] C.D. Taylor and D.V. Giri,*High-Power Microwave Systems and Effects*, Taylor and Francis, Washington DC, 1994, pp.167.
- [16] B.P. Dulla, "Development of a High Power Microwave (HPM) Advanced Concept Technology Demonstration (ACTD) for ASCM Defense of the ARG", Master's thesis, Naval Postgraduate School, December 1997.

- [17] N.J. Rudie, *Principles and Techniques of Radiation Hardening*, Vol.VIII, Western Periodicals Company, North Hollywood, 1986, p. 92-7.
- [18] N.J. Rudie, *Principles and Techniques of Radiation Hardening*, Vol.XII, Western Periodicals Company, North Hollywood, 1986, p. 139-1.
- [19] A.M. Todd et al., "Megawatt-class free electron laser concept for shipboard self-defense", SPIE, Vol.2988, pp.176-184.
- [20] R.A. Lyon, "Prime Power For Shipboard High-Average Power FELs", Master's Thesis, Naval Postgraduate School, December 1994.
- [21] A.M. Todd et al., "Megawatt-class free electron laser concept for shipboard self-defense", SPIE, Vol.2988, pp.176-184.
- [22] S. Benson, personal communication.
- [23] N.J. Rudie, *Principles and Techniques of Radiation Hardening*, Vol.XII, Western Periodicals Company, North Hollywood, 1986, p. 140-3.
- [24] J.R. Cook and J.R. Albertine, "The Navy's High Energy Laser Weapon System", SPIE, VOL.2988, pp264-271.
- [25] R.J. Lipinski, "Hole-Boring through Clouds for Laser Power Beaming", SPIE, Vol.2376, pp.2-10.
- [26] W.B. Colson, *Laser Handbook*, Vol. 6, Chapter 5, editors W.B. Colson, C. Pellegrini and A. Renieri, North-Holland, 1990, pp. 116-194.
- [27] K.E. Woehler, PH 4054 Course Notes, Naval Postgraduate School, 1998.
- [28] A. Cooper, personal communication.
- [29] L.K. Ang et al., "Surface instability of multipulse laser ablation on a metallic target", Journal of Applied Physics, April 1998, Vol.83, No.8.
- [30] E. Moshe et al., "An Increase of the spall strength in aluminum, copper, and Metglass at strain rates larger than 10^7 s^{-1} ", Journal of Applied Physics, April 1998, Vol.83, No.8.
- [31] J.T. Schriempf, Response of Materials to Laser Radiation: A Short Course, Naval Research Laboratory, Washington DC, July 1974.
- [32] R.F. Wenzel, "10.6 micron Pulsed Laser Penetration Studies on Aluminum", Proceedings of the 1980 DoD Conference on Laser Vulnerability, Effects, and Hardening, Vol.III, p.9. (SECRET document)

- [33] P.L. Eggins et al., "Multiple Pulse Laser Damage to CordonPreg (U)", Proceedings of the 1980 DoD Conference on Laser Vulnerability, Effects, Vol.III, p.57. (SECRET document)
- [34] S.I. Anisimov et al., "Electron emission from metal surfaces exposed to ultrashort laser pulses", Sov. Phys.-JETP, August 1974, Vol.39, No.2.
- [35] P.B. Allen, "Theory of Thermal Relaxation of Electrons in Metals", Physical Review Letters, September 1987, Vol.59, No.13.
- [36] H.E. Elsayed-Ali et al., "Time-Resolved Observation of Electron-Phonon Relaxation in Copper", Physical Review Letters, March 1987, Vol.58, No.12.
- [37] P.B. Corkum et al., "Thermal Response of Metals to Ultrashort-Pulse Laser Excitation", Physical Review Letters, December 1988, Vol.61, No.25.
- [38] M. Sparks, Journal of Applied Physics, 1976, Vol.47, p.837.
- [39] J.F. Figueira and S.J. Thomas, IEEE Journal of Quantum Electronics, 1982, Vol.18, p.1381.
- [40] P.B. Corkum et al., "Thermal Response of Metals to Ultrashort-Pulse Laser Excitation", Physical Review Letters, December 1988, Vol.61, No.25.
- [41] D. Du et al., "Laser-induced breakdown by impact ionization in SiO₂ with pulse widths from 7 ns to 150 fs", Applied Physics Letters, June 1994, Vol.64, No.23.
- [42] B.C. Stuart et al., "Laser-Induced Damage in Dielectrics with Nanosecond to Subpicosecond Pulses", Physical Review Letters, March 1987, Vol.74, No.12.

INITIAL DISTRIBUTION LIST

1. Defense Technical Information Center 2
8725 John J. Kingman Rd., STE 0944
Ft. Belvoir, Va 22060-6218
2. Dudley Knox Library 2
Naval Postgraduate School
441 Dyer Rd.
Monterey, CA 93943-5101
3. Professor William B. Colson, Code PH/Cw 4
Department of Physics
Naval Postgraduate School
Monterey, CA 93943-5117
4. Professor Robert L. Armstead, Code PH/Ar 1
Department of Physics
Naval Postgraduate School
Monterey, CA 93943-5117
5. Lieutenant Paul Herbert, USN 2
1664 HillCrest
Laguna Beach, CA 92651
6. John Albertine 1
109 Kingswood Rd.
Annapolis, MD 21401
7. Joung R. Cook 1
Research Physicist, Code 6655
Naval Research Laboratory
4555 Overlook Drive, SE
Washington, DC 20375-5000
8. Fred Dylla 1
TJNAF
12000 Jefferson Avenue
Newport News, VA 23606
9. George Neil 1
TJNAF
12000 Jefferson Avenue
Newport News, VA 23606